

4

FINAL REPORT

THE ROLE OF THERMOELASTIC EFFECTS  
IN THE SCUFFING FAILURE OF  
ROLLING/SLIDING EHD CONTACTS

Submitted to:

Department of the Navy  
Office of Naval Research  
Arlington, VA 22217-500

Report Submitted by:

R. R. Johnson and T. A. Dow  
Precision Engineering Laboratory  
Department of Mechanical and Aerospace Engineering  
North Carolina State University, Box 7910  
Raleigh, NC 27695-7910

For Work Performed Under Contract  
N00014-82-K-0551, Work Number 091-036

DIC  
AUG 25 1988  
H

15 August 1988

DISTRIBUTION STATEMENT A  
Approved for public release:  
Distribution Unlimited

#

ABSTRACT

A two-dimensional numerical solution of the thermal Reynolds', elasticity, and energy equations resulted in predictions of the flow velocities and temperatures within the lubricant film between a crown roller and a rotating shaft. The results showed a good agreement with previously measured experimental data on the surface temperatures in an EHD contact and on the resulting frictional torques for both rolling and sliding. A pressure and temperature dependent viscosity was assumed for the synthetic paraffinic hydrocarbon used in the experiments. This model allowed an evaluation of the relative importance of the generation, viscous dissipation, and compression terms in the energy equation at different stations along the mid-film line of contact. Based on the insight about the relative importance of terms as found in the numerical simulation, convenient expressions were developed for an approximate method of predicting the mid-film temperature and sliding friction force.

The influence of thermal expansion of the contact between a crowned surface in sliding contact with a rotating cylindrical surface was included in a model of thermoelastic instability to predict the onset of scuffing failure. The simplified approach assumed a heat balance between the generation from friction and the heat conducted into the cylinders. In addition it was assumed that elastic deformation caused by the thermal disturbance had the form of a cosine curve, and that the heat conduction into the rotating cylinder was one-dimensional. Results predicting the scuffing load at different sliding speeds showed reasonable agreement with previously reported experimental results. The scuffing load was quite sensitive to the value of the friction coefficient.

An experimental apparatus was built whereby the onset of scuffing could be observed for rolling/sliding contact between a crowned cylinder and a straight cylinder. Instrumentation included the means to measure speed, load, surface temperature near the contact spot, and frictional drag. The onset of scuffing was sensed by increased vibration or temperature. Experiments were performed using three contact lubricants of different rheology, and two steels with different thermal and material properties. Results correlate with the thermoelastic instability model in the regime of high calculated specific film thickness for the two steels tested.



Accession For	
NRL	<input checked="" type="checkbox"/>
DTIC TAB	<input type="checkbox"/>
Unannounced	<input type="checkbox"/>
Justification	
By <i>PER HP</i>	
Distribution/	
Availability Codes	
Dist	Special
<i>A-1</i>	

TABLE OF CONTENTS

	PAGE
ABSTRACT	
INTRODUCTION . . . . .	1
SUMMARY AND FUTURE WORK. . . . .	2
Two-dimensional Analysis of EHD Lubrication. . . . .	2
Approximate Analysis for Mid-Film Temperature and Sliding Friction Force . . . . .	3
Thermoelastic Stability Analysis . . . . .	3
DETAILS OF TECHNICAL PROGRAM . . . . .	5
Thermal Analysis of Elastohydrodynamic Lubrication in Rolling/Sliding Contacts . . . . .	5
Analytical Development. . . . .	5
Computational Scheme. . . . .	9
Results and Discussion of Numerical Solution. . . . .	10
An Approximate Method for Estimating Mid-Film Temperature and Sliding Friction Force in EHD Lubrication. . . . .	23
The Basis for the Approximation . . . . .	23
Governing Equations for Approximate Analysis. . . . .	24
The Approximate Analysis Compared with the More Complete Numerical Analysis. . . . .	30
Thermoelastic Instability in Elliptic Contact Between Two Cylinders Under Sliding Contact. . . . .	34
Conceptual Framework. . . . .	34
Theory and Analysis for a Simplified Case . . . . .	36
Results and Discussion of the Technique of the Simplified Case. . . . .	43
Experimental Testing of Failure due to Scuffing Apparatus Design. . . . .	46
Test Procedure. . . . .	48
Experimental Results. . . . .	50
Time Dependency of Failure. . . . .	51
Wear Observations . . . . .	56
Effects of Experimental Uncertainty . . . . .	56
REFERENCES . . . . .	57
APPENDIX A: LIST OF PARTICIPANTS, LIST OF PAPERS SUBMITTED FOR PRESENTATION OR PUBLICATION, LIST OF DEGREES GRANTED. . . . .	59

## LIST OF FIGURES

	PAGE
1 Velocity distribution in heavily loaded contacts.	8
2 Flow chart for computation scheme.	11
3 Dimensionless pressure and surface temperature variation through center of contact (970 N).	12
4 Dimensionless pressure and surface temperature variation through center of contact (454 N).	13
5 Temperature distribution through thickness of film (970 N).	15
6 Temperature distribution through thickness of film (454 N).	16
7 Shear in film (970 N).	18
8 Compression in film (970 N).	19
9 Conduction in film (970 N).	20
10 Convection (x-direction) in film (970 N).	21
11 Convection (y-direction) in film (970 N).	22
12 Heat generation and dissipation at the middle of the film (970 N).	25
13 Heat generation and dissipation at the middle of the film (454 N).	26
14 Pressure versus mid-film temperature.	31
15 Pressure versus sliding friction force.	33
16 Sliding velocity versus sliding friction force.	35
17 Geometry of the elliptical contact.	37
18 Geometry of contact region showing element of heat transfer analysis.	41
19 Comparison of calculated and measured scuffing loads for smooth and rough surfaces.	44
20 Comparison of calculated and measured scuffing loads with calculated friction coefficient.	47
21 Results of Test Group 1	52
22 Results of Test Group 2	53
23 Results of Test Group 3	54
24 Results of Test Group 4	55

## INTRODUCTION

The objective of the proposed program was to analyze the thermal effects in a rolling/sliding EHD contact to determine if they represent an important parameter leading to scuffing failure. A theoretical model determined the change in shape due to thermal expansion of the interacting surfaces as a result of non-uniform temperatures. The operating conditions and lubricant properties were studied to determine what situations are unstable; that is, which lead to more distortion and still higher heating.

Scuffing is a common mode of failure of lubricated contacts in gears, cam-followers seals, and other mechanisms which have a significant proportion of sliding in a load cycle. These mechanisms may be well supplied with lubricant, but the film thickness will be relatively small and the heat generation will be high because of the sliding. Scuffing failure occurs at small regions of the apparent contact area and typically consists of material transfer from the stationary member to the moving part. The transition to scuffing failure takes place after an initial period of operation during which little wear takes place and the friction coefficient is low. Failure is exhibited by a rapid increase in friction and high surface temperature, plus increased vertical vibration due to the transfer of material.

One explanation for such a failure relates to the thermal conditions in the contact and their effect on the lubrication. The transition period may be a period of heating and distorting the contact such that high pressure and temperatures reduce the film thickness or high temperatures reduce or eliminate the effectiveness of the boundary lubricants

The research program explored the possibility that thermal effects in an EHD contact can distort the surfaces to produce unstable heating; that is, local heating will produce a change in surface shape that will lead to still higher heating in that region. The research involved critical analysis and experiments to determine if such an explanation could be applied to scuffing failures. The results which demonstrated the validity of this hypothesis show that the analysis can serve as a basis for material property and operating conditions selection to avoid the occurrence of this failure mode.

The research is organized in a series of steps or tasks that will ultimately determine the validity of the hypothesis that a thermoelastic instability can give rise to scuffing. A thermal analysis of EHD lubrication in rolling and sliding contacts has been carried out and is described in this report, as is an elementary analysis of thermoelastic instability for a simplified case. These two steps have been followed by an experimental evaluation and a more detailed thermoelastic instability analysis using the thermal EHD model. Results of the work done are presented in the sections that follow.

## SUMMARY

The efforts over this reporting period have concentrated on three aspects. The first was the continued development of a two-dimensional numerical solution to the thermal problem of elastohydrodynamic lubrication of rolling/sliding contacts. The second has been the simplified formulation of a thermoelastic instability theory applied to the case of thermal expansion effects of a stationary crowned surface in sliding contact with a rotating cylindrical surface. The third has been the design and testing of an apparatus to experimentally investigate the onset of scuffing and its relation to load, speed, and local temperature. The overall goal is to understand the role that thermal effects play in elastohydrodynamic lubrication and eventual failure of the contact.

## Two-Dimensional Analysis of EHD Lubrication

A two-dimensional numerical solution of the thermal Reynolds' elasticity, and energy equations resulted in predictions of the flow velocities and temperatures within the lubricant film between a crown roller and a rotating shaft. The results showed a good agreement with previously measured experimental data on the surface temperatures in an EHD contact and on the resulting frictional torques for both rolling and sliding. A pressure and temperature dependent viscosity was assumed for the synthetic paraffinic hydrocarbon used in the experiments. This model allowed an evaluation of the relative importance of the generation, viscous dissipation, and compression terms in the energy equation at different stations along the mid-film line of contact. Based on the insight about the relative importance of terms as found in the numerical simulation, convenient expressions were developed for an approximate method of predicting the mid-film temperature and sliding friction force.

The following conclusions were drawn:

1. For pure rolling conditions the compression heating is the major contributor to the increase of temperature in the contact zone.
2. There is significant increase in film temperature as the slip is increased.
3. The contribution of convection in the y-direction is significant in the inlet zone.
4. For slip conditions the major sources of heat generation and dissipation are the shear and conduction.
5. For slip conditions as the load increases the contribution of compression and convection in the x-direction increase.
6. For slip conditions the maximum temperature occurs at the mid-film at a point where the pressure is at its greatest and  $dP/dx = 0$ .

### Approximate Analysis for Estimating Mid-Film Temperature and Sliding Friction Force

An approximate solution to the problem of thermal elastohydrodynamic lubrication of sliding contacts is obtained. An equation for the mid-film temperature which is a function of viscosity, fluid conductivity, sliding velocity, and temperature viscosity exponent is obtained. The shear stress on the disk surface over the contact region is also obtained. The following conclusions were drawn:

1. The maximum temperature rise occurs at the middle of the film at the point where  $dP/dx = 0$ .
2. There is significant increase in the film temperature as the slip is increased.
3. For slip conditions the major sources of heat generation and dissipation are the shear and conduction.
4. The mid-film temperature increases linearly as the load is increased.
5. For a given load, the traction force initially rises with sliding speed, reaches a maximum, then drops with further increases in speed.
6. The results for the mid-film temperature and sliding traction force obtained from FDA [4] and the approximate solution indicate excellent correlation exists between the results.

### Thermoelastic Stability Analysis

Thermoelastic instability in an elliptic contact between a straight and crowned cylinder is suggested as a potential initiator of scuffing failure. An approximate equation is presented as a guide to delineate the region of instability. The agreement of the calculated results with the available experimental data is satisfactory.

Since this is a simplified approach, some assumptions are made, such as the elastic deformation caused by the thermal disturbance being in the form of cosine curve, and the conduction at the surface of the rotating cylinder is one dimensional. Further theoretical analysis is being performed to examine the thermoelastic instability theory.

### Experimental Tests of Scuffing

An experimental apparatus has been built whereby the onset of scuffing may be observed. Instrumentation includes the measurement of speed, load, surface temperature near the contact spot, and frictional drag. The onset of scuffing can be sensed by increased vibration or temperature. The experimental results can be summarized as follows:

1. The theoretical scuffing model is viable in the regime of high calculated specific film thickness ( $\lambda > 4$ ) for steels having different thermal properties.
2. The model fails to adequately predict scuffing in the regime of low calculated values of specific film thickness ( $\lambda < 1.3$ ).
3. Although the theoretical model predicts a response to variation in thermal and material properties, the experimental results did not answer the question as to whether the difference exists or not.
4. A time dependency to failure was observed in the regime of high calculated specific film thickness. The trend has not been quantified but is found to agree with the observations in other research.
5. Some indications of moving hot spots were observed.

## DETAILS OF TECHNICAL PROGRAM

During this program three areas of research have been pursued. The first was the continued development of a two-dimensional numerical solution to the thermal problem of elastohydrodynamic lubrication of rolling/sliding contacts. The second has been the simplified formulation of a thermoelastic instability theory applied to the case of thermal expansion effects of a stationary crowned surface in sliding contact with a rotating cylindrical surface. The third has been the design and testing of an apparatus to experimentally investigate the onset of scuffing and its relation to load, speed and local temperature.

## Thermal Analysis of Elastohydrodynamic Lubrication in Rolling/Sliding Contacts

A two dimensional numerical solution to the problem of thermal elastohydrodynamic lubrication of rolling/sliding contacts was obtained using a finite difference formulation. The technique involves the simultaneous solution of the thermal Reynold's equation, and the two dimensional energy equation. A pressure and temperature dependent viscosity for a synthetic paraffinic hydrocarbon (XRM-109F) was considered in the solution of the Reynolds' and energy equations. The experimental pressure and surface temperature measurements obtained by Dow and Kannel [1] were used in evaluating the results of the numerical analysis for the cases of pure rolling and slip conditions.

Analytical Development

Solution of the two dimensional thermal elastohydrodynamic lubrication problem requires the simultaneous solution of the thermal Reynold' equation, the energy equation with the fluid properties as functions of pressure and temperature, and the elasticity equation.

The thermal Reynolds' equation is obtained from the principles of conservation of mass and momentum applied to an element of the lubricant. The following assumptions have been made in the development of the governing equations.

1. The viscosity of the lubricant is only a function of pressure and temperature (not dependent on the shear rate).
2. The body and the inertia forces are negligible in comparison to the pressure and viscous forces.
3. The radii of curvature of rolling elements are much larger than the lubricant film thickness. Therefore, all effects due to curvature of the fluid film are neglected.
4. The pressure is constant across the thickness of the film.
5. Thermal conductivity, specific heat, and thermal expansibility do not vary with pressure or temperature.

Using the foregoing assumptions, the thermal Reynolds' equation, can be written as:

$$\frac{\partial}{\partial x} (G_2 \frac{dP}{dx}) = u_1 \frac{\partial}{\partial x} (G_3) + \frac{\partial}{\partial x} \left[ \frac{G_1}{u_{e0}} (u_2 - u_1) \right] \quad (1)$$

where

$$G_1 = \int_0^h \int_0^y \left( \int_0^y \frac{dy}{u} \right) dy \quad (2)$$

$$G_2 = \frac{u_{e1}}{u_{e0}} G_1 - \int_0^h \int_0^y \left( \int_0^y \frac{y}{u} \right) dy \quad (3)$$

$$G_3 = \int_0^h dy \quad (4)$$

$$u_{e0} = \int_0^h \frac{dy}{u} \quad (5)$$

$$u_{e1} = \int_0^h \frac{y}{u} dy \quad (6)$$

The temperature field within the lubricant film is obtained from the solution of the energy equation. Neglecting the heat conduction in the direction of flow, the energy equation may be written as:

$$\rho_f c_f \left( u \frac{\partial T}{\partial x} + \frac{\partial T}{\partial y} \right) = u \left( \frac{\partial u}{\partial y} \right)^2 + \hat{R} T u \frac{\partial P}{\partial x} + k_f \frac{\partial^2 T}{\partial y^2} \quad (7)$$

where

$$u = \frac{dP}{dx} \int_0^y \frac{y}{u} dy + \left[ \frac{u_2 - u_1}{u_{e0}} - \frac{u_e dP/dx}{u_{e0}} \right] \int_0^y \frac{dy}{u} + u_1 \quad (8)$$

$$\frac{\partial u}{\partial y} = \frac{1}{u} \left[ \frac{dP}{dx} \left( y - \frac{u_{e1}}{u_{e0}} \right) + \frac{u_2 - u_1}{u_{e0}} \right] \quad (9)$$

The energy equation (7) requires two boundary conditions for its solution (temperature on the surface of each rolling element). The experimental surface temperature measurements [1] were used as the boundary conditions for the calculation of the temperature field.

The pressure distributions from the experimental measurements [1] at the center of the the contact width closely resemble the elliptical Hertzian pressure distribution. Therefore, the inlet zone film shape is assumed to be that of the Hertz equation of dry line contact.

$$h = \left( \frac{1 - \nu_1^2}{E_1} + \frac{1 - \nu_2^2}{E_2} \right) P_{\max} a \left\{ \frac{x}{a} \left[ \frac{x^2}{a^2} - 1 \right]^{-1/2} - \ln \left[ \frac{x}{a} + \left[ \frac{x^2}{a^2} - 1 \right]^{1/2} \right] \right\} \quad (10)$$

The Hertz equation (10) is used to calculate the film shape outside the contact zone. The film thickness inside the contact zone is calculated from the thermal Reynolds' equation (1).

The viscosity/pressure relationship used in this analysis was proposed by Roelands [2];

$$\log \mu = (\log \mu_0 + 1.2) \left( 1 + \frac{P}{2000} \right)^{-1.2} \quad (11)$$

An exponential change of viscosity with temperature was incorporated and the complete viscosity relationship can be expressed as:

$$\mu = \frac{10 [(\log \mu_0 + 1.2) \left( 1 + \frac{P}{2000} \right)^{-1.2}]}{e^{\lambda(T - T_s)}} \quad (12)$$

The lubricant under investigation was a synthetic paraffinic hydrocarbon.

The velocity profile in the x-direction obtained from the equilibrium of an infinitesimal element is given by equation (8). The velocity profile in the y-direction (across the film) could be obtained from the continuity equation:

$$\frac{\partial u}{\partial x} + \frac{\partial v}{\partial y} = 0 \quad (13)$$

This equation is a first order partial differential equation needing only one boundary equation for its solution. However, the geometry of an EHD regime illustrated in Figure 1 provides two boundary conditions. If the continuity equation is differentiated with respect to y the following is obtained.

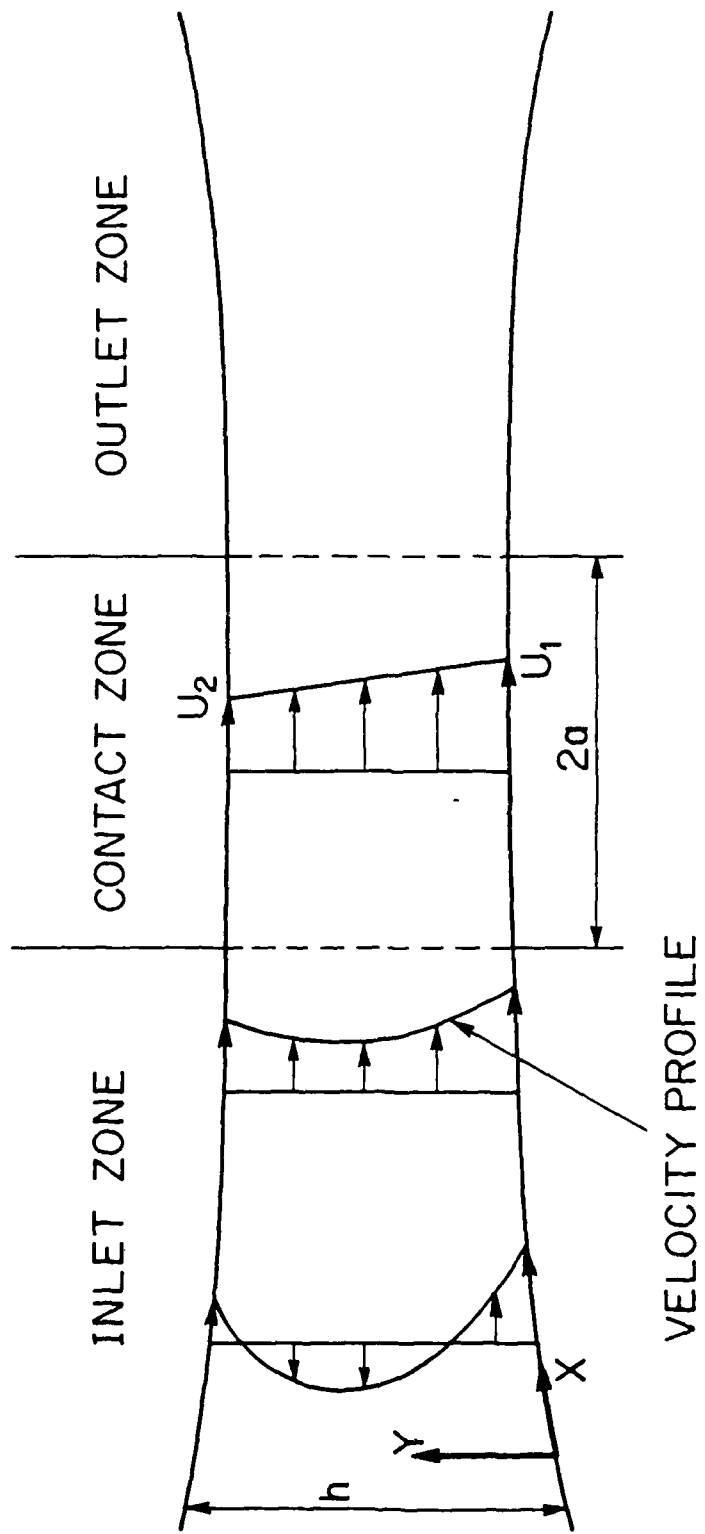


Figure 1. Velocity distribution in heavily loaded contacts

$$\frac{\partial^2 v}{\partial y^2} = -\frac{\lambda}{\lambda y} \left( \frac{\partial u}{\partial x} \right) \quad (14)$$

This equation is a second order partial differential equation needing two boundary conditions, which are readily available from the surface velocities of the disks. Equation (14) is used to evaluate velocity in the y-direction using finite difference formulation. Figure 1 illustrates the variation of velocity in the rolling direction; backflow occurs in the inlet zone and becomes a positive linear flow at the center of the contact where the pressure gradient is zero.

#### Computational Scheme

In order to solve the thermal elastohydrodynamic lubrication problem, the isothermal case is solved first. The results obtained from the isothermal case are then used as initial solution for the thermal case. The isothermal equations can easily be obtained from the thermal equations by allowing the viscosity of the lubricant to be a function of pressure and independent of temperature.

The differential equations (1) and (7) were replaced by their equivalent finite difference formulation. An iterative solution of the momentum and energy equations is used to determine the shear stress, the velocities in the x and y-directions, and the temperature profile throughout the inlet and contact zone for prescribed boundary conditions. The results of the isothermal case are then used in conjunction with the energy equation to calculate the initial temperature field within the lubricant film. The effects of this temperature distribution are introduced on the viscosity, film shape, and fluid flow in the x and y-directions. These values are then used to calculate a new temperature field. This iterative procedure is continued until the temperature field reaches steady state. The rheological properties of the lubricant are allowed to vary as a function of local pressure and temperature.

One of the main difficulties in solving fluid dynamic problems involving the Navier Stokes and energy equations, is the appearance of nonlinear substantial derivatives. These derivatives require a knowledge of the flow direction at each node before they can be evaluated. A formalized method of handling such problems is to utilize the "upwind" differencing scheme [3]. The temperature at each surface node is known from measured surface temperatures. It is also assumed to be ambient at the entry nodes where the x-component of velocity, u is positive. If the flow field predicts backflow at some entry nodes, the temperature at these nodes are dependent values and must be found during the numerical solution. The major difference between the "upwind" differencing scheme and other solution schemes lies in the use of upwind values to define a convect flux. The local velocities in the x and y-directions are defined from equations (8) and (14). If the flow is positive the downwind value for the temperature at node (i,j) is assumed; and if the flow is negative the upwind value is assumed for that node. A number of subroutines have been constructed for the evaluation of the temperature field within the

lubricant film. These subroutines provide information such a transient viscosity, viscosity integrals, etc. Values are recalculated using these subroutines after each temperature field is obtained. The fluid integrals (equations (2), (3), (5), and (6)) were evaluated using the trapezoidal rule.

The flow chart of Figure 2 illustrates the computational procedure that was used for calculating the temperature field within the lubricant film. The isothermal viscosity of the lubricant (equation (11)), film shape (equation 10), and velocity in the x and y-direction (equations (8) and (14)) are calculated based on the measured pressure and surface temperature data. These values are used to arrive at the initial temperature field. The calculated temperature field is then used to introduce the influence of temperature on the viscosity and a new flow field is calculated. The iteration procedure is continued until the lubricant temperature obtained from the energy equation (7) does not change from one iteration to the next. One aspect of the solution technique is the limitation on the temperature change per iteration. This procedure was designed to speed convergence and involves limiting the temperature change which can occur for a flow field iteration. The final temperature distribution is the same with or without using a limited temperature change, but convergence is reached considerably faster when the limiting temperature is used. Using the limitation that the temperature change will be less than or equal to 10% of the current temperature, the energy equation can be solved in 15-20 iterations.

#### Results and Discussion of Numerical Solution

Figures 3 and 4 illustrate the experimental pressure and surface temperature measurements obtained by Dow and Kannel [1] using a rolling disk machine with a synthetic paraffinic oil. Figures 3a and 3b depict pressure and surface temperature for pure rolling and 6.2% slip condition for a disk load of 970N. The dimensions and the properties of the rolling disk machine and lubricant are tabulated in Table 1. Figure 3a indicates that the peak surface temperature for pure rolling occurs in the inlet zone near the point of maximum pressure gradient. For the case of 6.2% slip the peak surface temperature has moved toward the center of the contact where the pressure is maximum. Figure 4 illustrates the measured pressure and surface temperature at 454 N of disk load for pure rolling and 5.3% slip condition. For the pure rolling (Figure 4a), peak surface temperature rise is 12° C. above the ambient and occurs in the inlet zone near the peak pressure gradient as it did of for the 970N load. For the case of 5.3% slip (Figure 4b), the temperature peak has again moved towards the center of the contact to the point of maximum pressure as in the case of 6.2% slip at 970 N disk load. These experimental measurements were used as the boundary conditions for the solution of thermal Reynolds' equation, and the two dimensional heat equation.

Figures 5 and 6 illustrate the calculated temperature distribution through the thickness of the lubricant film resulting from the effects of shear, compression, conduction, and convection in the x and y-directions. For pure rolling condition (Figure 5a), the peak lubricant temperature rise in the film is 36° C. above the ambient whereas the peak surface

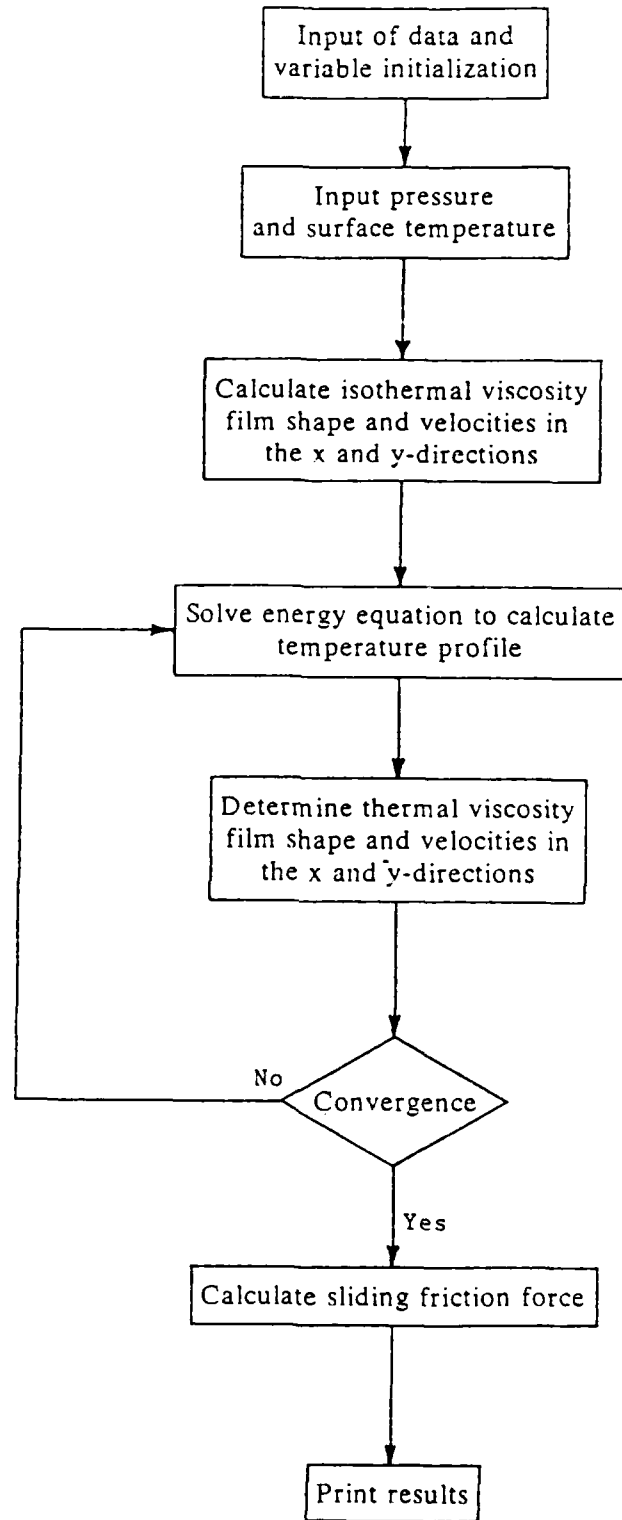
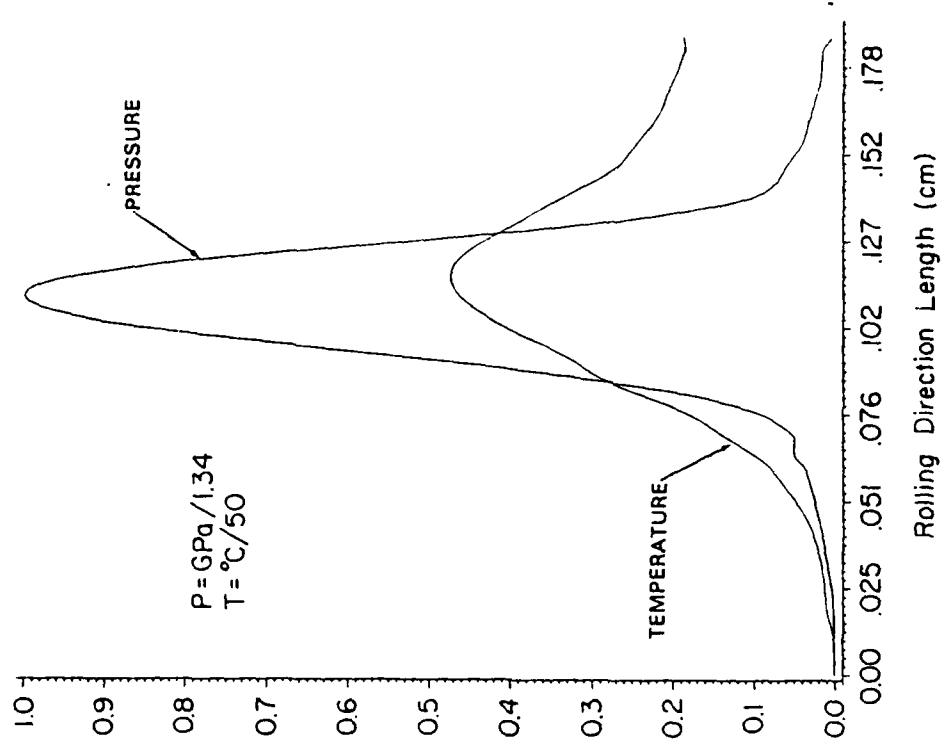
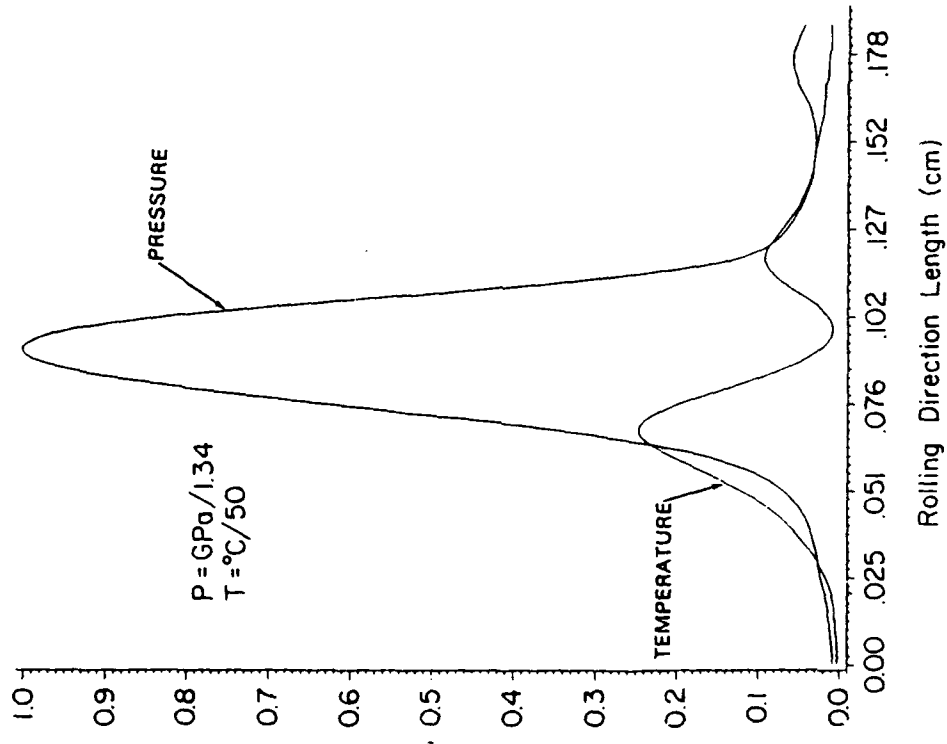


Figure 2. Flow Chart for Computation Scheme



a) Pure rolling condition



b) 6.2% slip condition

Figure 3. Dimensionless pressure and surface temperature variation through the center of contact (970 N).

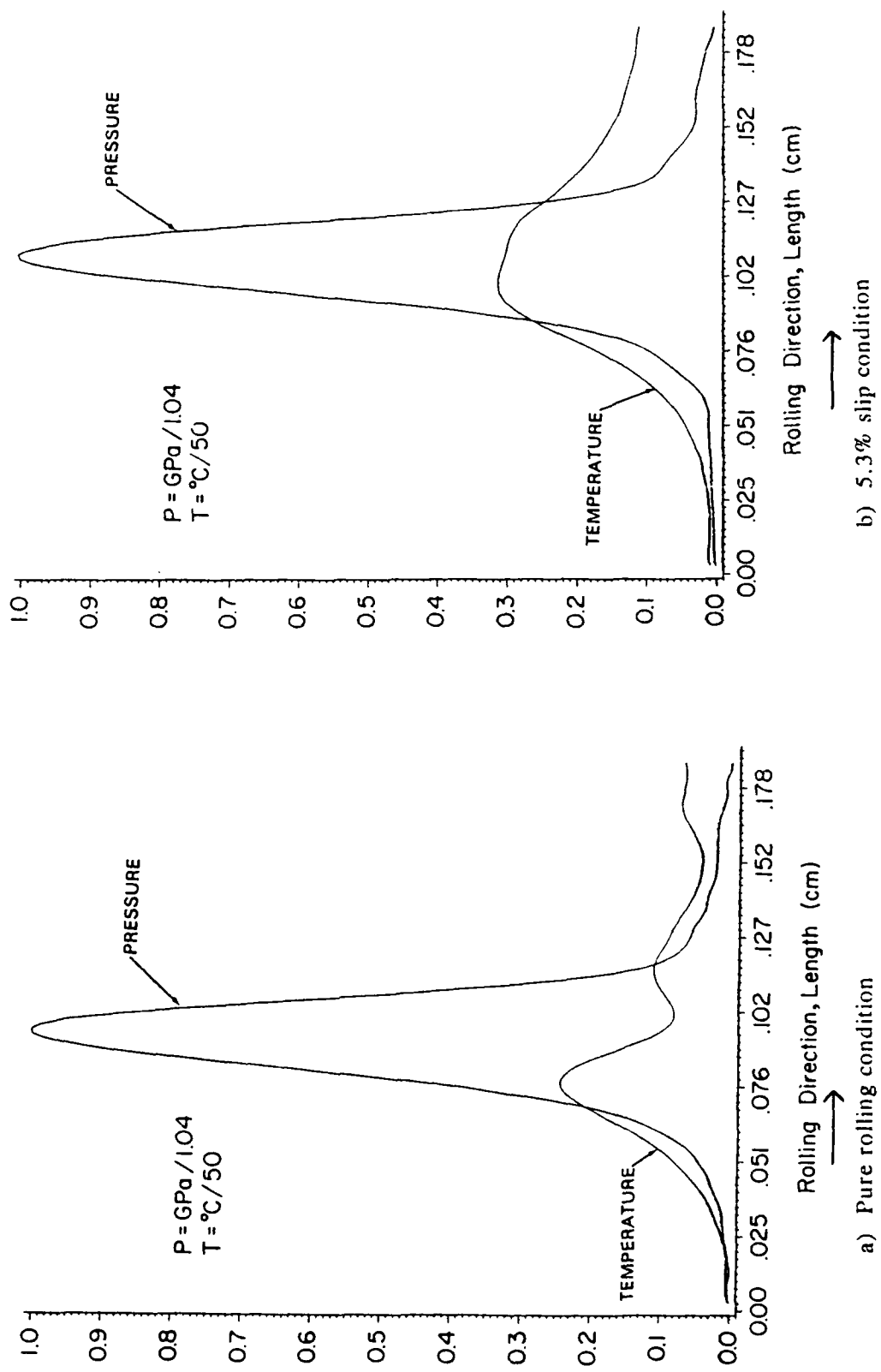
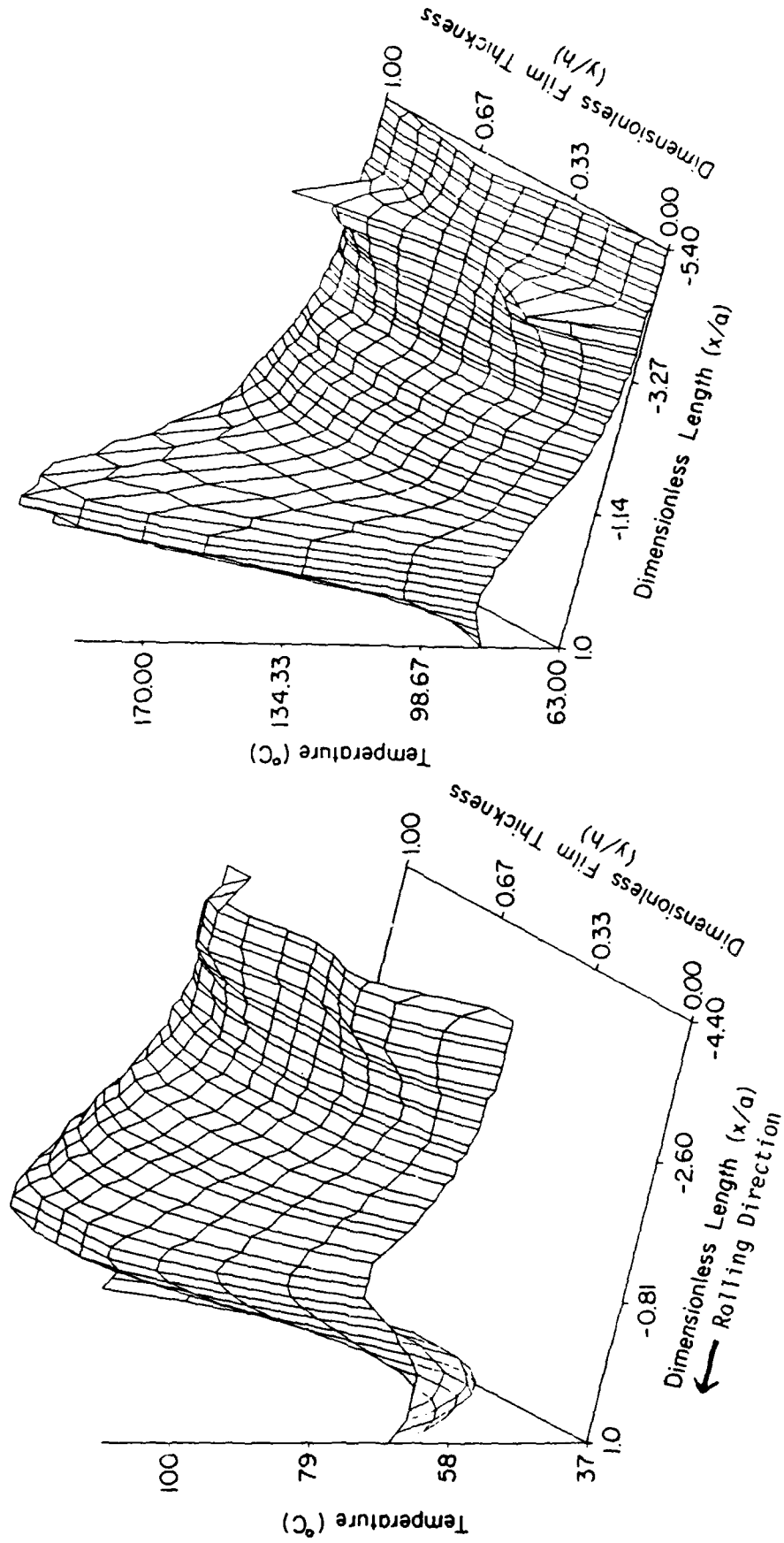


Figure 4. Dimensionless pressure and surface temperature through the center of contact. (454 N).

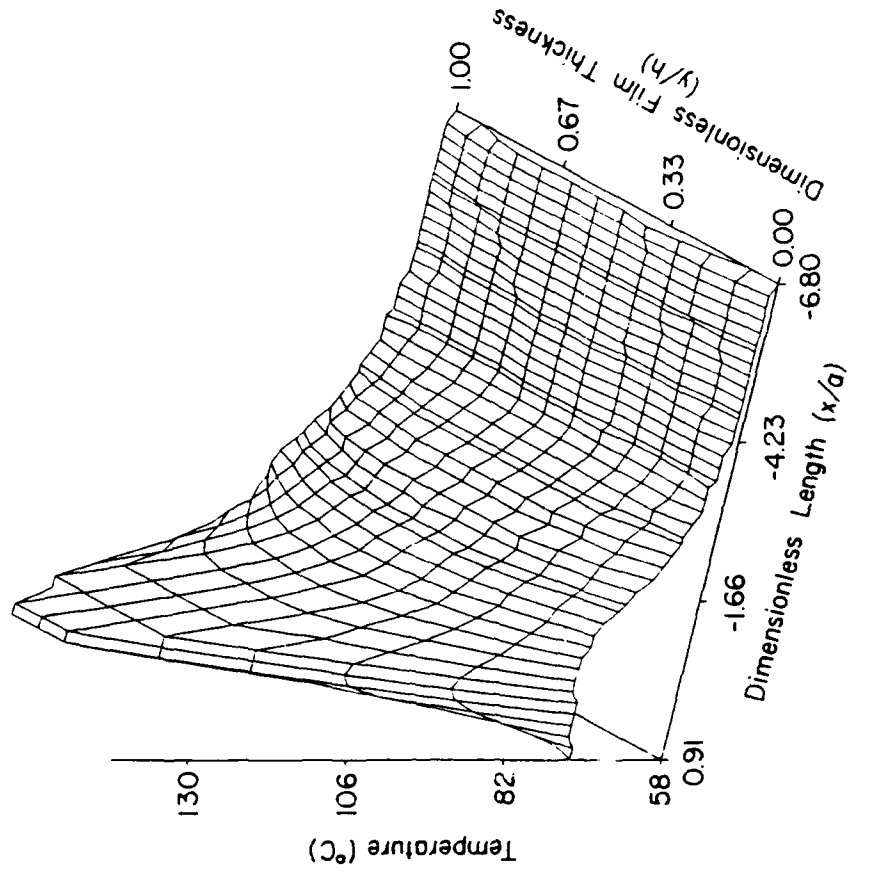
Table 1. Disk and lubricant properties

Material of both disks	steel
Lubricant synthetic paraffinic hydrocarbon	XRM-109F
Diameters of upper disk, cm	3.569
Diameter of lower disk, cm	3.546
Crown radius of lower disk, cm	20.569
Rotational speed (nominal), rad/sec	525
Surface speed (nominal), cm/sec	934.7
Specific heat of the disk times the density, $\text{KJ}/(\text{m}^3 \text{ } ^\circ\text{C})$	3723
Thermal conductivity of the disk, $\text{W}/(\text{m } ^\circ\text{C})$	27.22
Modulus of elasticity of the disks, GPa	207
Poisson's ratio of the disks	.3
Thermal conductivity of the lubricant, $\text{W}/(\text{m } ^\circ\text{C})$	240
Specific heat of the lubricant times the density, $\text{KJ}/(\text{m}^3 \text{ } ^\circ\text{C})$	1744
Thermal viscosity coefficient, $1/ \text{ } ^\circ\text{C}$	.04
Thermal expansivity of the lubricant, $1/ \text{ } ^\circ\text{C}$	.00069
Exponent for Roeland's viscosity model	.45

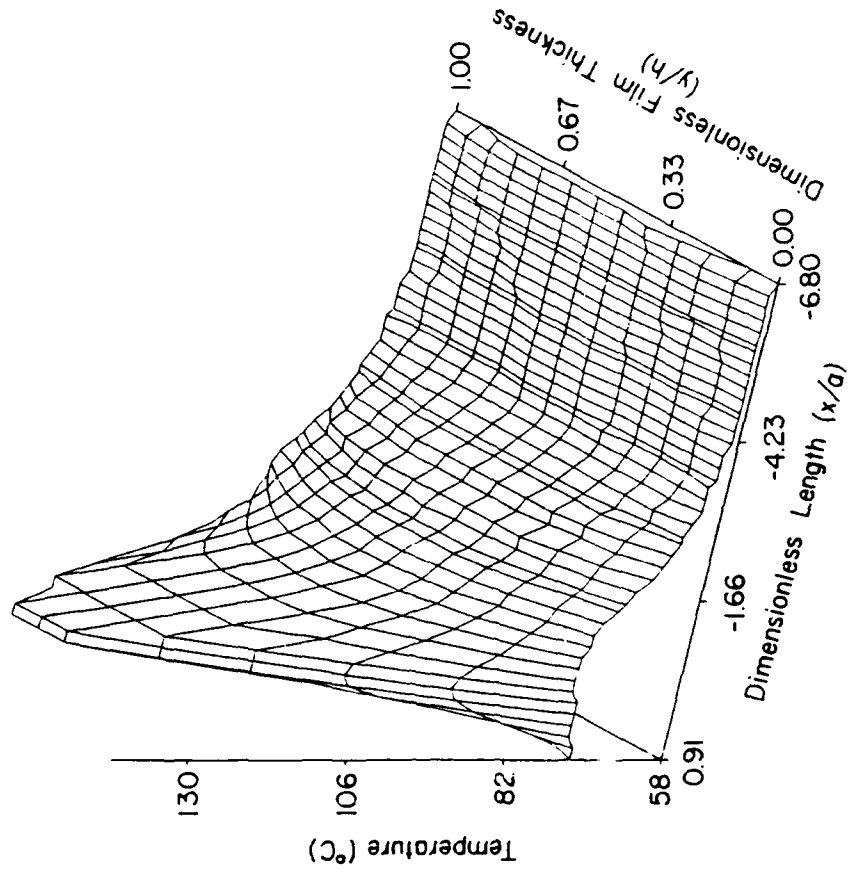


a) Pure rolling condition  
b) 6.2% slip condition

Figure 5. Temperature distribution through the thickness of the film (97C N).



a) Pure rolling condition



b) 5.3% slip condition

Figure 6. Temperature distribution through the thickness of the film (454 N)

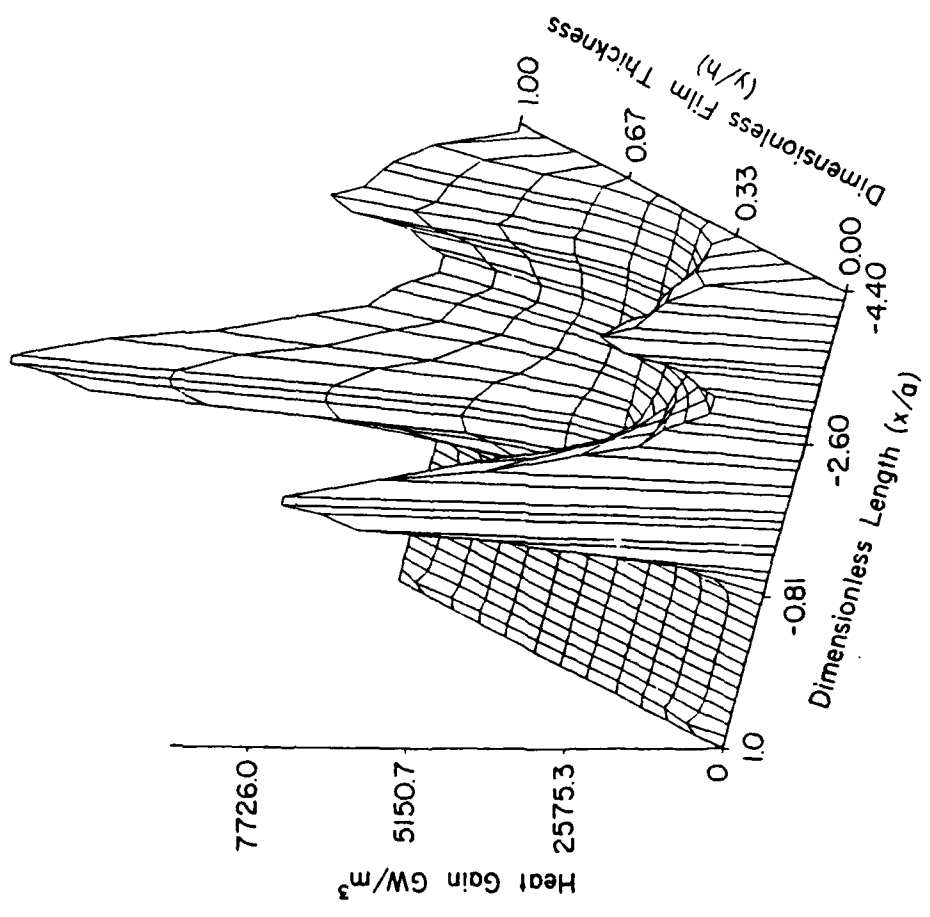
temperature is  $13^{\circ}$  C. above the ambient. For the 6.2% slip case Figure 5b, the peak temperature in the film is  $110^{\circ}$  C. above the ambient for a surface peak of  $24^{\circ}$  C. above the ambient. It is important to note that the lubricant film temperature rise for the pure rolling condition mainly occurs in the inlet zone. Whereas for the slip condition the rise occurs in the contact zone. The temperature rise for pure rolling condition is moderate, but significant temperature increase occurs for the slip condition. Figure 6 depicts the temperature distribution for pure rolling and 5.3% slip condition at 454 N of disk load. Again in this case, as in the case of 970 N disk load, significant temperature rise occurs at the mid-film for the 5.3% slip condition. The mid-film temperature (Figure 6b) rises to  $72^{\circ}$  C. above ambient compared to the surface temperature rise of  $16^{\circ}$  C. above ambient.

Figures 7 through 11 illustrate the component of heat generation and dissipation for pure rolling and 6.2% slip conditions at a disk load of 970 N. Close study of these components reveals the significance of each and the location of its maximum.

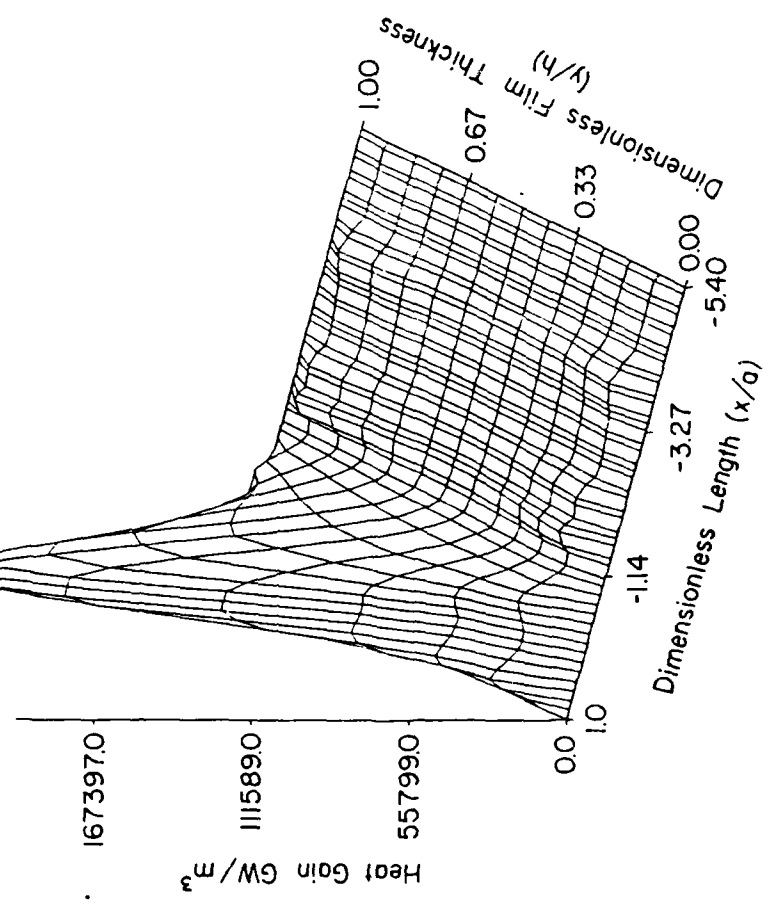
Figure 7 illustrates the component of heat generation due to shear. For the pure rolling condition (Figure 7a) all of the shear heating is generated in the inlet zone near the disk surface. The shear heating is maximum at the disk surface and gradually decreases to its minimum of zero at the middle of the film. The shear heating is zero in the contact zone; because the gradient of velocity is zero in this region for pure rolling conditions. The maximum value of shear heating occurs at the surface of the disks near the entrance to the contact zone. Figure 7b depicts the shear heating for 6.2% slip. For this case, in contrast of pure rolling, most of the shear heating occurs in the high pressure region (contact zone). The maximum value is 22 times greater than that of the pure rolling condition. Significant shear heating also occurs in the inlet zone, but compared to the peak value it does not appear large on the graph.

Figure 8 illustrates the magnitude and distribution of the heat generated by compression in the lubricant film. Compressive heating is proportional to the pressure gradient, and as a result it will be the same across the thickness of the film. The heating will also be similar for pure rolling and slip conditions; because of their similar pressure distributions. Comparing the magnitude of the heat generated by shear (Figure 7) and compression (Figure 8) indicates that shear heating plays a dominant role in the temperature rise across the fluid film for slip conditions but is similar to compressive heating for pure rolling conditions.

The component of heat loss due to conduction is presented in Figure 9. Conduction heat loss is proportional to the second derivative of temperature across the film as well as the coefficient of thermal conductivity of the lubricant. It is instructive to compare the heating due to shear (Figure 7) and that due to compression (Figure 8) with the heat loss due to conduction shown in Figure 9. The peak value of conduction for pure rolling is essentially all the heat generated due to compression. For this case the shear heating is small. Figure 9b depicts the conduction loss for the 6.2% slip condition. As in the case

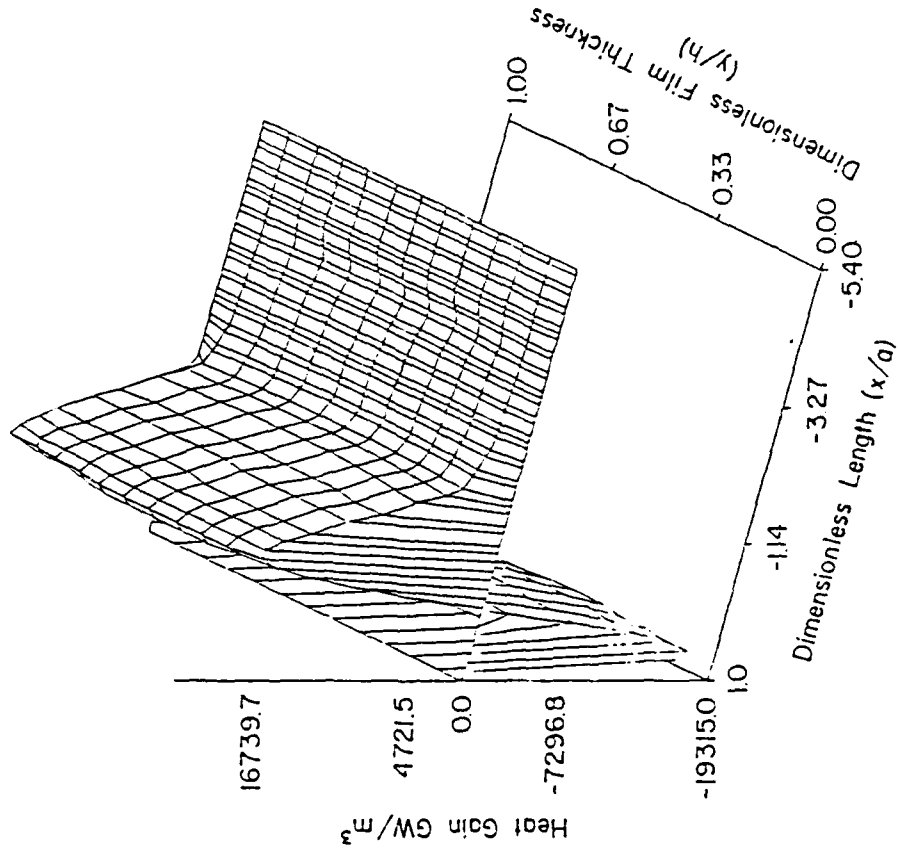


a) Pure rolling condition

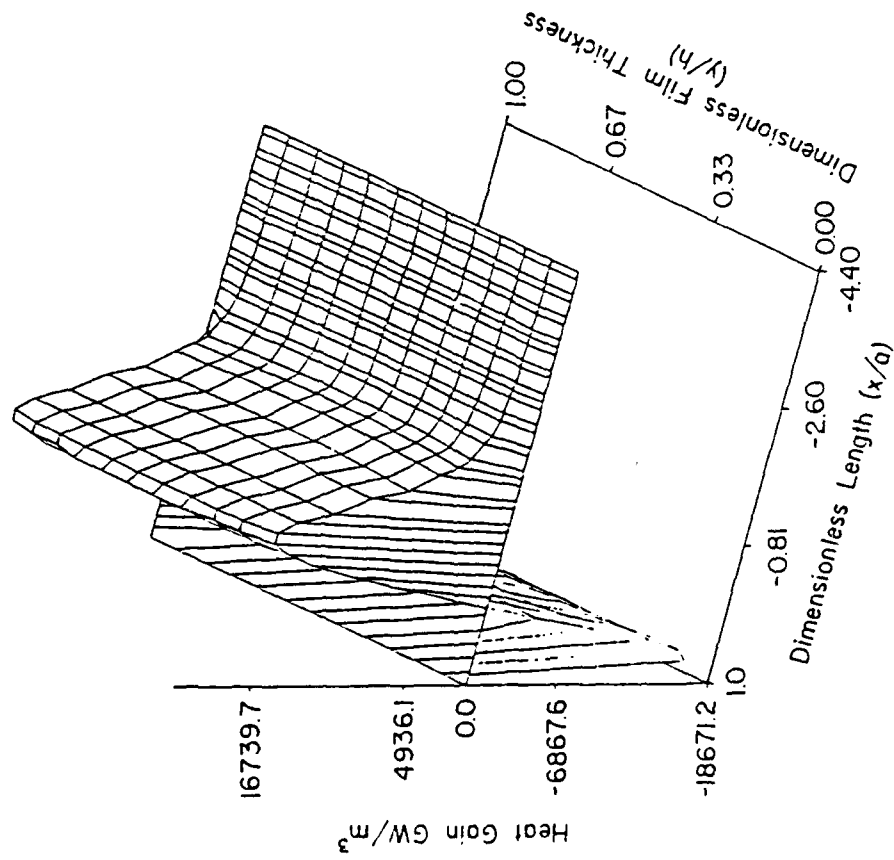


b) 6.2% slip condition

Figure 7. Heat generated due to shear in film (970 N)

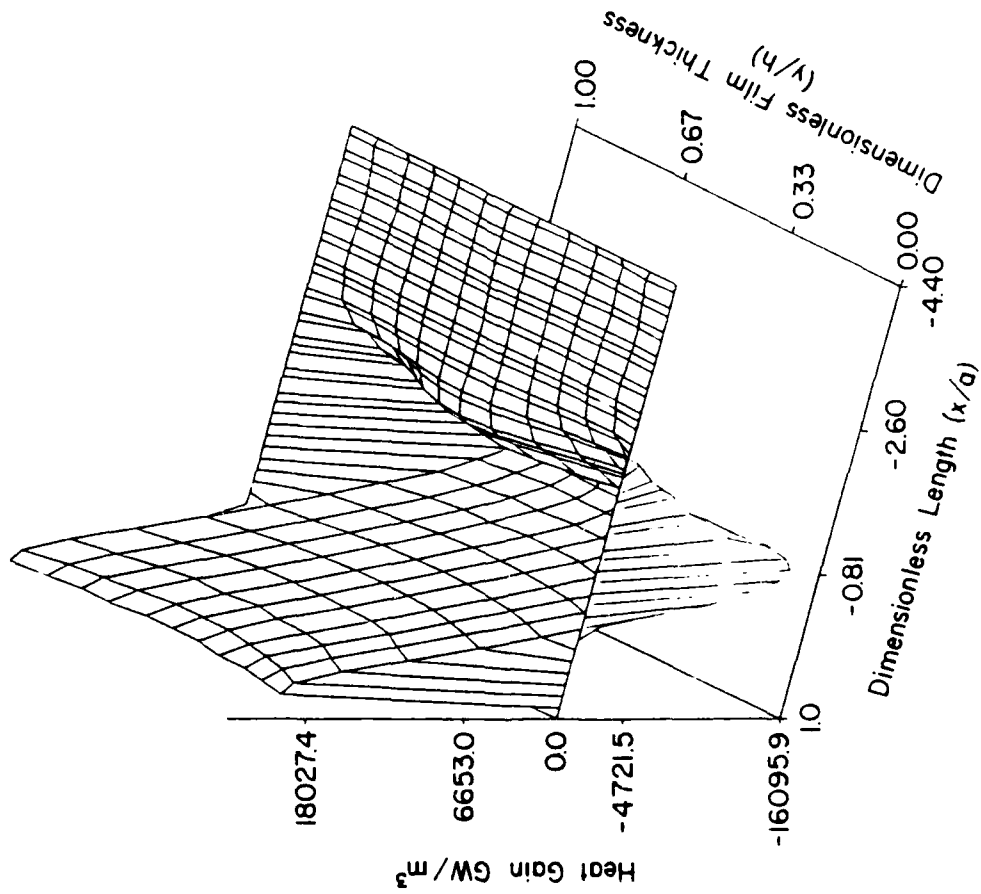


a) Pure rolling condition

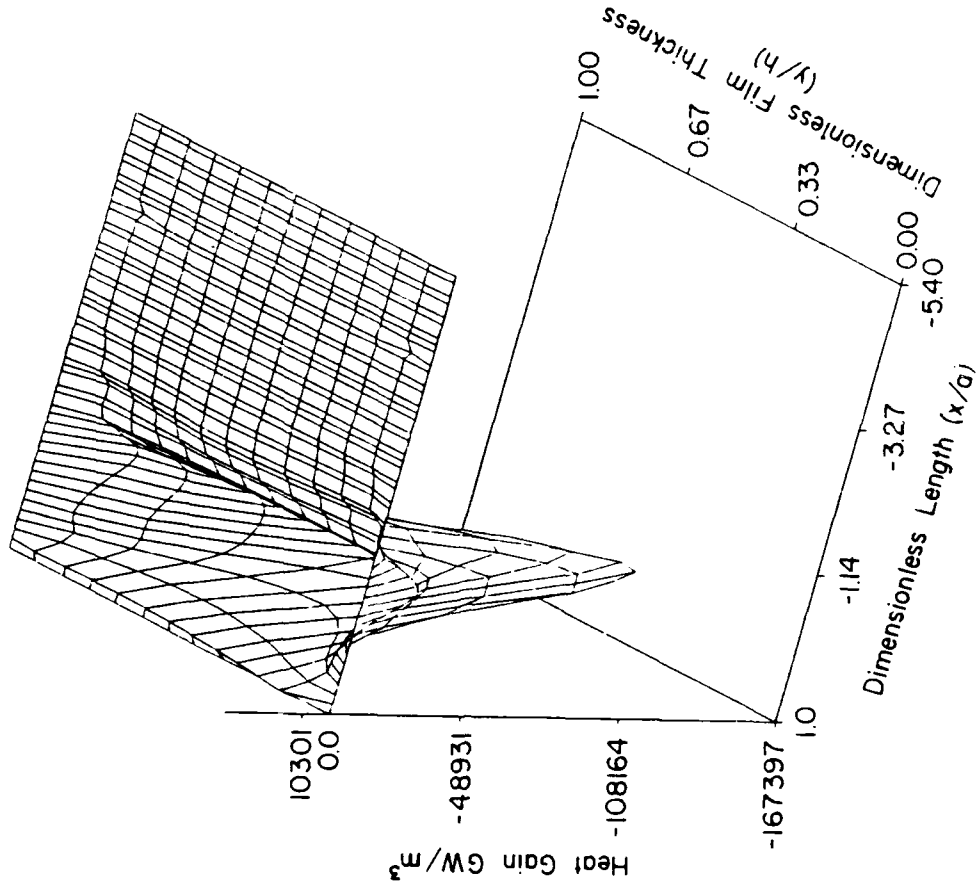


b) 6.2% slip condition

Figure 8. Heat generated due to compression in the film (970 N)

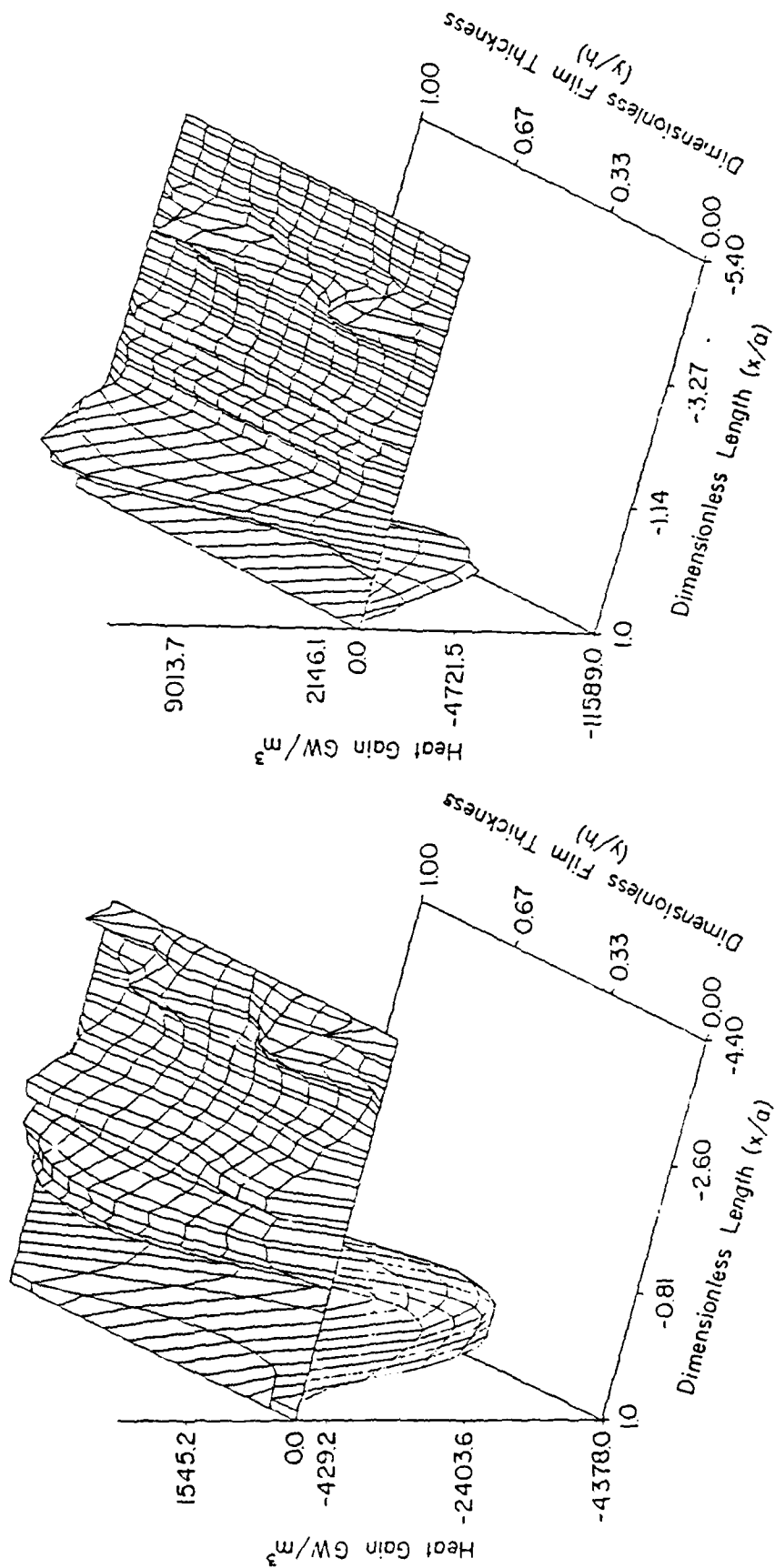


a) Pure rolling condition



b) 6.2% slip condition

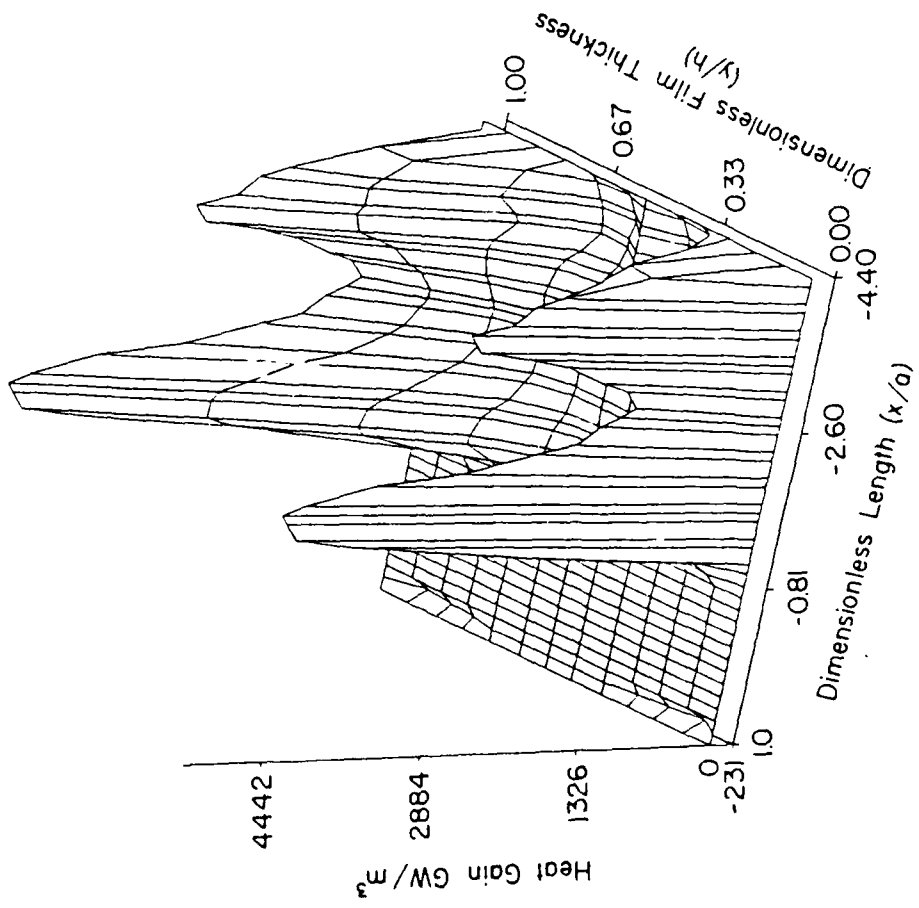
Figure 9. Heat loss due to conduction in the film (970 N)



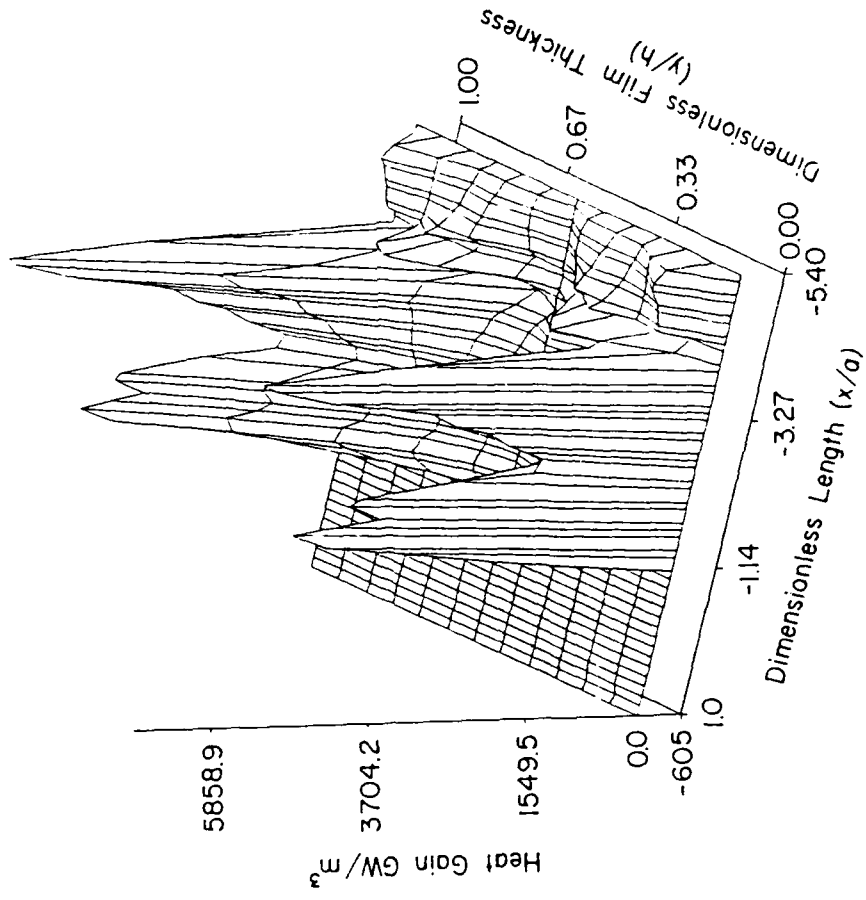
a) Pure rolling condition

b) 6.2% slip condition

Figure 10. Heat loss due to convection (x-direction) in the film (970 N)



a) Pure rolling condition



a) 6.2% slip condition

Figure 11. Heat loss due to convection (y-direction) in the film (970 N)

of pure rolling condition, conduction is the dominant mode of heat transfer; however, for this case the conduction heat loss in the contact zone appears identical to the shear heating gain in the film (Figure 7b) since the compressive heating is negligibly small.

Convection heat loss in the x-direction (rolling direction) is proportional to the fluid density, specific heat, velocity in the x-direction, and the gradient of temperature in the x-direction. The convection peaks at the mid-film in the center of the contact, where the velocity and the gradient of temperature are the greatest. Figure 10 illustrates the convection heat loss in the x-direction. Even though for pure rolling (Figure 10a) the maximum convection is 1/4 of that due to conduction; its contribution cannot be neglected. Figure 10b depicts the convection in the x-direction for 6.2% slip. Its magnitude is much larger than those of pure rolling as the change in scale indicates.

Figure 11 illustrates the component of heat loss due to convection in the y-direction (across the film). This convection is also proportional to fluid density, specific heat, velocity in the y-direction, and the gradient of temperature in the y-direction. The velocity in the y-direction has its maximum at the boundaries and gradually decreases to zero at the mid-film for pure rolling, and at a point close to mid-film for slip conditions. This convection term reaches its maximum of (Figure 11a) at the boundary in the inlet zone where the velocity in the y-direction is the greatest. It is zero at the mid-film and in the contact zone where the boundaries are nearly parallel. Figure 11b depicts the convection in the y-direction for 6.2% slip. It has a maximum value at the boundary as in the case of pure rolling and goes to zero at a point near the middle of the film. Close study of this term reveals its contribution is only in the inlet zone, and has no effect on the temperature in the contact zone and can thus be neglected.

#### An Approximate Method for Estimating Mid-Film Temperature and Sliding Friction Force in EHD Lubrication

An approximate method for estimating mid-film temperature and sliding friction force in elastohydrodynamic (EHD) lubrication of sliding contacts has been obtained. The calculation is an approximation based on the conditions at the point of maximum pressure where  $dP/dx = 0$ , but the results indicate excellent correlation exists between this approximate method and results of the more comprehensive analysis presented in the last section.

#### Basis for the Approximation

The results of the last section (to be published in ASME Journal of Tribology [4]) can be used to calculate the temperature in an EHD fluid film. This solution takes into account the conduction, convection in both x and y-directions, shear and compression. It illustrates the temperature rise in sliding conditions and extensively investigates the contribution of each component of the heat generation and dissipation. The results obtained indicated that the maximum temperature rise occurs

at the middle of the film. Therefore, it is of interest to compare the magnitude of heat generation and dissipation at the middle of the film. Figure 12 represents these terms at the middle of the film for pure and 6.2% slip condition at a disk load of 9 ton. For the pure rolling condition (Figure 12a) it is observed that the convection in the y-direction and shear have no influence on the heat balance in the middle of the film. The major contributors are the compression and conduction. Although, convection in the x-direction removes heat from the contact; its influence is much smaller than that of conduction. Figure 12b depicts the generation and dissipation terms at the same disk load at 6.2% slip. In this case, in contrast to pure conditions, the major contributor to the temperature rise in the film is shear heating. The major loss term is the conduction. Though, the compression and convection in the x-direction are not negligible, as a first approximation only the shear and conduction need be considered.

Figure 13 illustrates the heat generation and dissipation at 454 N disk load for pure rolling and 5.3% slip condition. This figure confirms the conclusion made from the higher load condition previously discussed, namely, for slip conditions the shear is the major heat source and the conduction is the major heat sink. However, the contribution of compression and convection in the x-direction are less significant in this load than at the 970 N load. Therefore, the components of compression and convection in the x and y-direction in the middle of the film could be neglected. Thus, the predominant modes of heat generation and dissipation are the shear and conduction. This conclusion is used as the basis for an approximate solution to the problem of thermal EHD lubrication.

#### Governing Equations for the Approximate Analysis

Assuming that the predominant terms in the film are the shear heating and conduction heat loss, the energy equation (1) can be obtained from the heat balance on an elemental control volume.

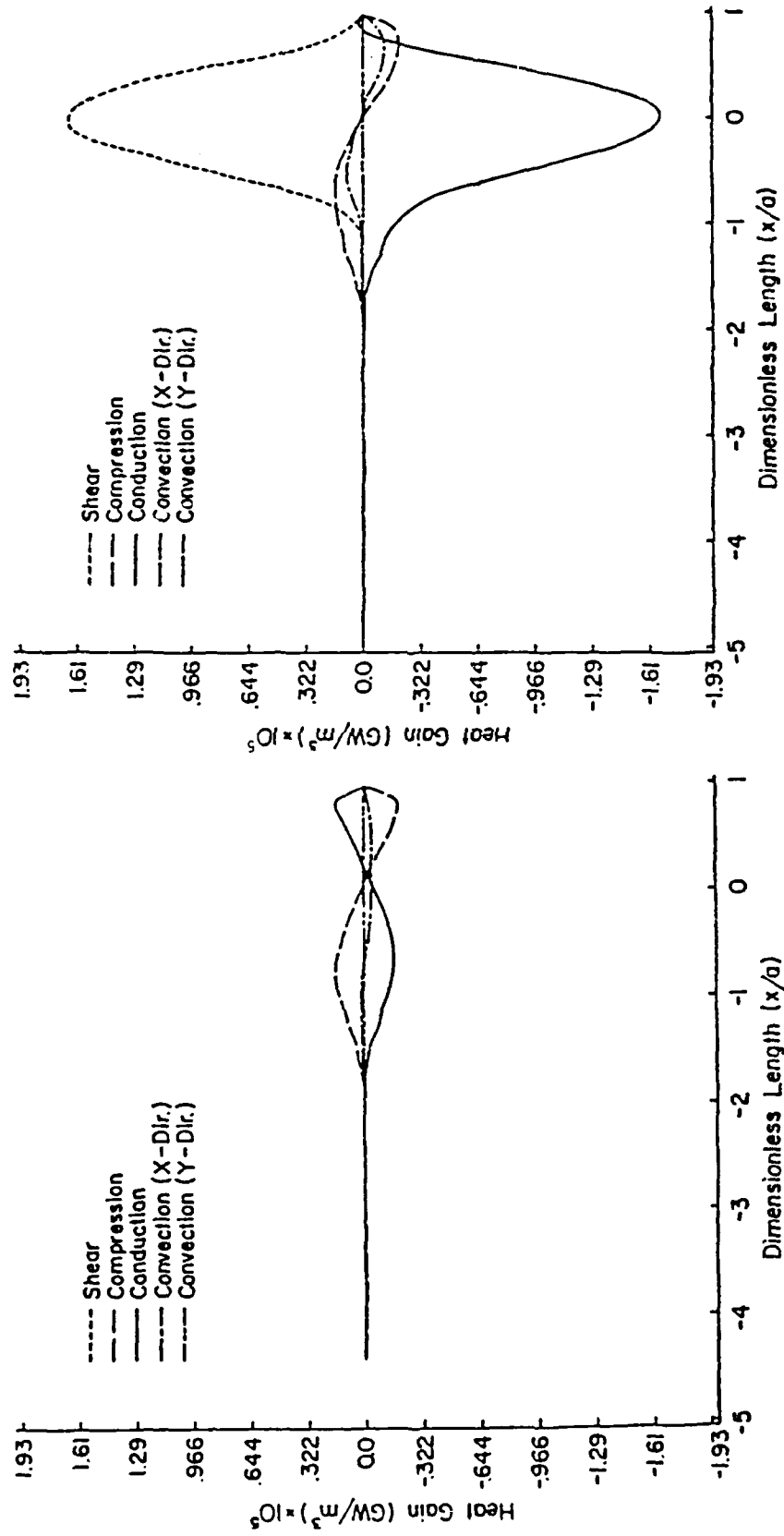
$$\rho c \left( u \frac{\partial T}{\partial x} + v \frac{\partial T}{\partial y} \right) = \mu \left( \frac{\partial u}{\partial y} \right)^2 + \beta T U \frac{\partial P}{\partial x} + K_f \frac{\partial^2 T}{\partial y^2} \quad (1)$$

If compression heating and convection of heat along and across the film (x and y-directions respectively) can be neglected, then the energy equation for a Newtonian lubricant model can be written as:

$$K_f \frac{\partial^2 T}{\partial y^2} = - \mu \left( \frac{\partial u}{\partial y} \right)^2 \quad (2)$$

Rewriting in terms of shear stress, equation (2) may be written as:

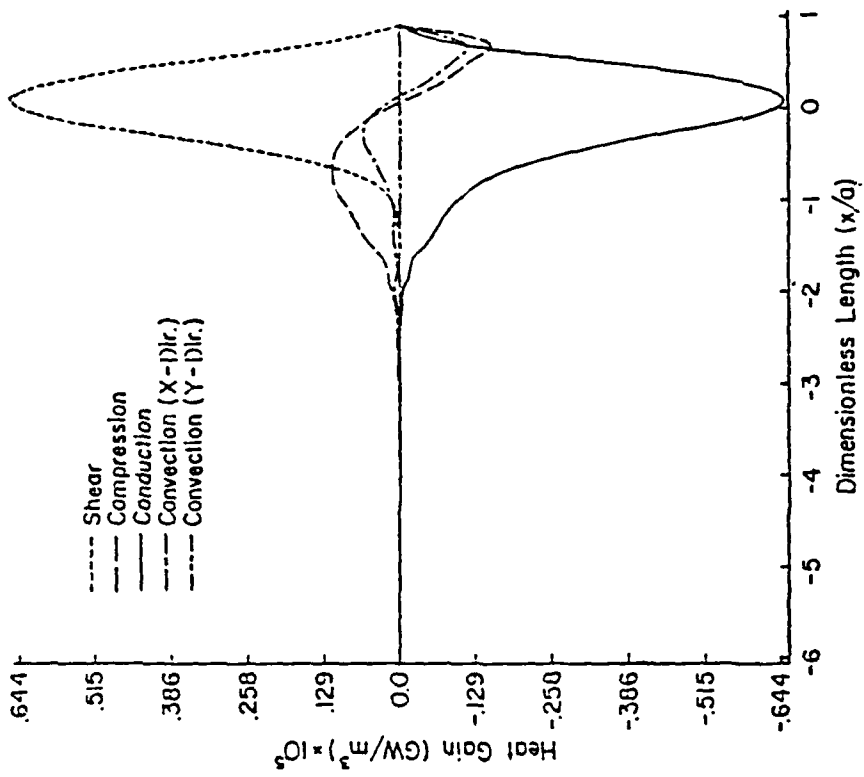
$$\frac{\partial^2 T}{\partial y^2} = - \frac{\tau^2}{\mu K_f} \quad (3)$$



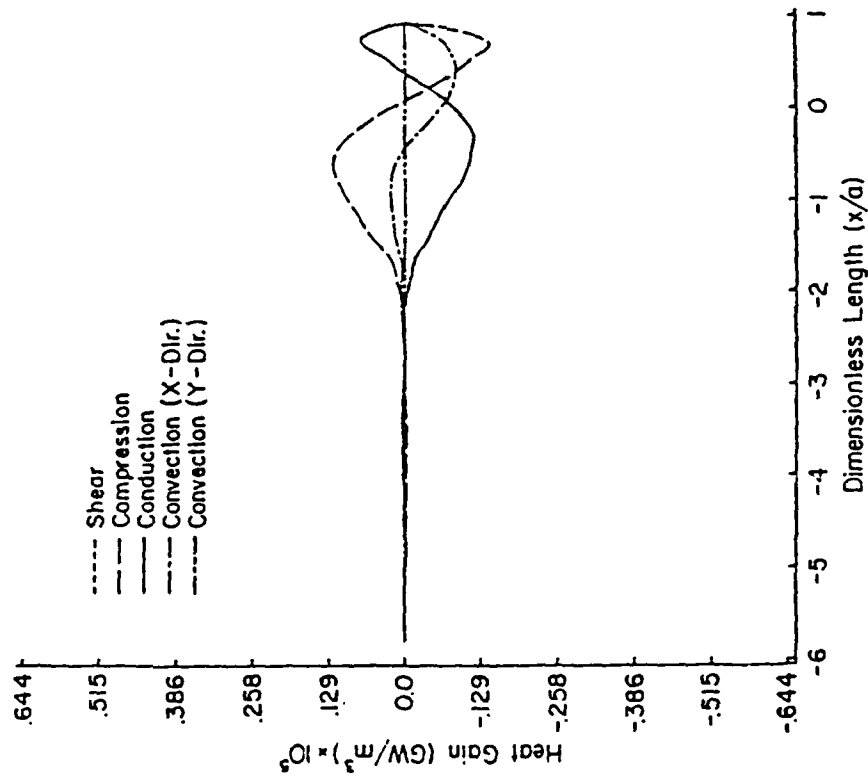
a) Pure rolling condition

b) 6.2% slip condition

Figure 12. Heat generation and dissipation at the mid-film (970 N)



a) Pure rolling condition



b) 5.3% slip condition.

Figure 13. Heat generation and dissipation at the mid-film (454 N)

The Roelands' viscosity model [6] including the temperature effect is given by:

$$\mu = \frac{10^{[(\log \mu_0 + 1.2)(1 + P/28400)^2 - 1.2]}}{e^{\delta T}} \quad (4)$$

For convenience the numerator will be represented by  $\mu(P)$ . Substituting for viscosity in equation (3) results in:

$$\frac{\partial^2 T}{\partial y^2} = -\frac{\tau^2 e^{\delta T}}{K_f \mu(P)} \quad (5)$$

This equation can be easily integrated with respect to  $y$  if the shear stress ( $\tau$ ) is constant with respect to  $y$ . This condition exists at the peak pressure. It was observed from the analysis that the maximum temperature occurs at the point of maximum pressure, where  $dP/dx = 0$ . The basic relation for the equilibrium of an element in an EHD lubrication contact is given by equation (6).

$$\frac{dp}{dx} = \frac{\partial \tau}{\partial y} \quad (6)$$

Evaluating this equation at the point of maximum pressure results in:

$$\frac{dp}{dx} = 0 \quad (7)$$

hence,

$$\frac{\partial \tau}{\partial y} = 0 \quad (8)$$

Therefore,  $\tau$  is constant with respect to  $y$ . The rest of the analysis presented here is thus only valid at  $dP/dx = 0$ . Integrating equation (5) the following is obtained.

$$\left(\frac{\partial T}{\partial y}\right)^2 = \frac{-2\tau^2 e^{\delta T}}{K_f \delta \mu(P)} + c_1 \quad (9)$$

In order to evaluate  $c_1$ , define the position where

$$\frac{\partial T}{\partial y} = 0 \quad \text{at } y = y_c \quad (10)$$

Where  $0 < y_c < h$ , also at  $y = y_c$ ,  $T = T_c$ , and  $\mu = \mu_c$ . Hence the constant is:

$$c_1 = \frac{2 \tau^2 e^{\delta T_c}}{K_f \delta \mu(P)} \quad (11)$$

Substituting  $c_1$  in equation (9) results in;

$$\frac{\partial T}{\partial y} = \pm \tau \left( \frac{2e^{\delta T_c}}{K_f \delta u(P)} \right)^{1/2} \left( 1 - \frac{e^{\delta T}}{e^{\delta T_c}} \right)^{1/2} \quad (12)$$

Let

$$\Lambda = \frac{e^{\delta T}}{e^{\delta T_c}} \quad (13)$$

and

$$\Lambda = \tau \left( \frac{2e^{\delta T_c}}{K_f \delta u(P)} \right)^{1/2} \quad (14)$$

Therefore,

$$\frac{\partial T}{\partial y} = \pm \Lambda (1 - \Lambda)^{1/2} \quad (15)$$

rearranging the above equation results in the following.

$$\frac{dT}{(1 - \Lambda)^{1/2}} = \pm \Lambda dy \quad (16)$$

Differentiating equation (13) with respect to T results in:

$$dT = \frac{d\Lambda}{\delta \Lambda} \quad (17)$$

Substituting equation (17) into equation (16) and integrating:

$$\Lambda y = \pm \frac{1}{\delta} \int \frac{d\Lambda}{\Lambda (1 - \Lambda)^{1/2}} \quad (18)$$

The boundary conditions are;  $T = T_1$  at  $y = 0$  and  $T = T_2$  at  $y = h$  and  $T = T_c$  at  $y = y_c$ . Integrating equation (18) between  $y = 0$  and  $y = y_c$  the following is obtained.

$$\Lambda y_c = \pm \frac{1}{\delta} \int_{\Lambda_1}^{\Lambda} \frac{d\Lambda}{\Lambda (1 - \Lambda)^{1/2}} \quad (19)$$

letting

$$\psi = \int_{s_1}^1 \frac{d\lambda}{\lambda (1 - \lambda)^{1/2}} \quad (20)$$

Substituting  $\lambda$  and  $\psi$  in equation (19) and assuming both surface temperatures to be equal to  $T_g$ , the shear stress expression becomes,

$$\tau = \frac{\psi}{h} \left( \frac{2K_f \mu(P)}{\delta e^{\delta T_c}} \right)^{1/2} \quad (21)$$

Equation (21) describes the shear stress present in the contact. The friction force is obtained by multiplying this shear stress by the area of the contact. The length of the contact area for the approximate solution is the length of the high pressure regions, where the shear stress is determined. Equation (21) requires an estimate of mid-film (y-direction) temperature therefore, this temperature is developed next.

From the Newtonian lubricant model assumption the velocity gradient could be written as:

$$\frac{\partial u}{\partial y} = \frac{\tau}{\mu} = \frac{\tau e^{\delta T}}{\mu(P)} \quad (22)$$

Rearranging the temperature gradient equation (12) the following is obtained.

$$dy = \frac{\pm dT}{\tau \left( \frac{2e^{\delta T_c}}{K_f \delta \mu(P)} \right)^{1/2} \left( 1 - \frac{e^{\delta T}}{e^{\delta T_c}} \right)^{1/2}} \quad (23)$$

Combining equations (22) and (23) to eliminate  $dy$ :

$$du = \frac{\pm \tau e^{\delta T} dT}{\tau \mu(P) \left( \frac{2e^{\delta T_c}}{K_f \delta \mu(P)} \right)^{1/2} \left( 1 - \frac{e^{\delta T}}{e^{\delta T_c}} \right)^{1/2}} \quad (24)$$

Integrating this equation yields:

$$u = \pm \left( \frac{2K_f e^{\delta T_c}}{\delta \mu(P)} \right)^{1/2} (1 - \lambda)^{1/2} + c'_z \quad (25)$$

Using the boundary conditions at  $y = 0$ ,  $u = u_1$ ,  $T = T_1$ , and at  $y = h$ ,  $u = u_2$  and  $T = T_2$ , results in:

$$u_2 - u_1 = \left( \frac{2K_f e^{\delta T_c}}{\delta u(P)} \right)^{1/2} \left[ \left( 1 - \frac{e^{\delta T_{s2}}}{e^{\delta T_c}} \right)^{1/2} + \left( 1 - \frac{e^{\delta T_{s1}}}{e^{\delta T_c}} \right)^{1/2} \right] \quad (26)$$

This equation allows  $T_c$  to be calculated in terms of the boundary conditions  $u_2$  and  $u_1$ . Letting  $T_1 = T_2 = T_s$  in equation (26). The following is obtained.

$$T_c = \frac{1}{\kappa} \ln \left[ e^{\delta T_s} + \frac{\delta (u_2 - u_1)^2 u(P)}{8 K_f} \right] \quad (27)$$

Equation (27) predicts the temperature at the mid-film at the point of maximum pressure and  $dP/dx = 0$ . Figure 14 compares the mid-film temperature above ambient at  $dP/dx = 0$ , obtained from the finite difference analysis (FDA) [4] and equation (27) as a function of maximum Hertz pressure for different slip ratios. It illustrates that as the pressure increases (load increases), the maximum film temperature increases linearly. Figure 14 illustrates that the approximate temperature equation (27) predicts values of mid-film temperature, which are 4% higher than those obtained from FDA [4]. This high prediction is mainly due to the neglect of convection in the x-direction. It is also apparent that good correlation exists between the results obtained from FDA [4] and the approximate solution of equation (27).

The mid-film temperature equation (27) depends on the temperature at the surface of the disk. However, the surface temperature  $T_s$ , is typically unknown. Table 2 contains the mid-film temperature obtained from equation (27) when surface temperature was retained and when neglected. Table 2 indicates that the contribution of  $T_s$  in equation (27) may be neglected thus reducing to:

$$T_c = \frac{1}{\delta} \ln \left[ \frac{\delta (u_2 - u_1)^2 u(P)}{8 K_f} \right] \quad (28)$$

Table 2 also contains the mid-film temperature obtained from the FDA [4]. The comparison indicates that equation (28) does not correlate well with the results from FDA [4] and equation (27) at low pressures and low slip conditions. However, as the pressure is increased at a particular sliding velocity the predictability of equation (28) greatly improves. The accuracy also increases as sliding velocity is increased.

#### The Approximate Analysis Compared with the More Complete Numerical Analysis

The variation of sliding friction force equation (21) with pressure is illustrated in Figure 15. The increase in pressure, results in an increase in sliding force at a constant sliding velocity. This is a

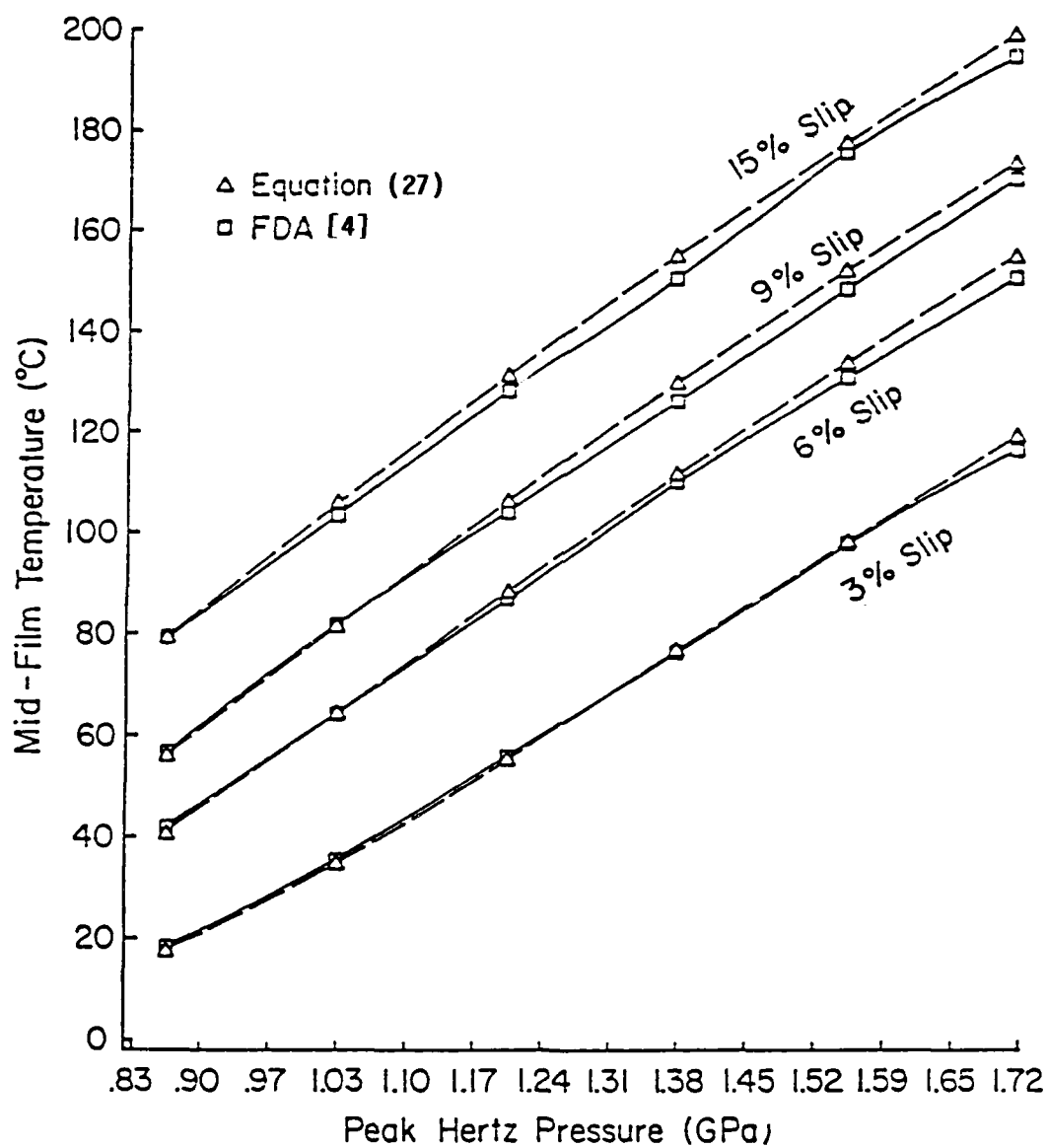


Figure 14. Peak Hertz pressure versus mid-film temperature

Table 2. Results obtained from equation (27), equation (28), and FDA (4).

Pressure GPa	Equation (27) 3% slip C	Equation (28) 3% slip C	FDA[4] 3% slip C	Equation (27) 6% slip C	Equation (28) 6% slip C	FDA [4] 6% slip C
.8619	17.73	-3.60	18.22	40.87	32.70	41.94
1.034	34.79	24.42	35.64	64.35	60.72	64.33
1.207	55.32	50.36	56.00	88.32	86.66	86.84
1.379	77.01	74.59	76.36	111.68	110.89	110.23
1.551	98.61	97.41	98.04	134.09	133.70	131.05
1.724	119.63	119.01	116.89	155.51	155.31	151.04
1.896	139.91	139.58	135.90	175.98	175.87	172.87
1.965	147.80	147.54	144.16	183.92	183.84	179.92

Pressure GPa	Equation (27) 9% slip C	Equation (28) 9% slip C	FDA [4] 9% slip C	Equation (27) 15% slip C	Equation (28) 15% slip C	FDA[4] 15% slip C
.8619	56.13	51.33	56.76	79.15	76.88	79.15
1.034	81.43	79.36	81.81	105.87	104.90	103.45
1.207	106.23	105.29	104.19	131.27	130.83	128.22
1.379	129.98	129.52	126.34	155.28	155.06	150.77
1.551	152.56	152.34	148.78	177.99	177.88	176.17
1.724	174.06	173.94	170.92	199.54	199.48	195.30
1.896	194.57	194.51	189.31	220.08	220.05	217.22
1.965	202.52	202.47	198.11	228.04	228.01	224.65

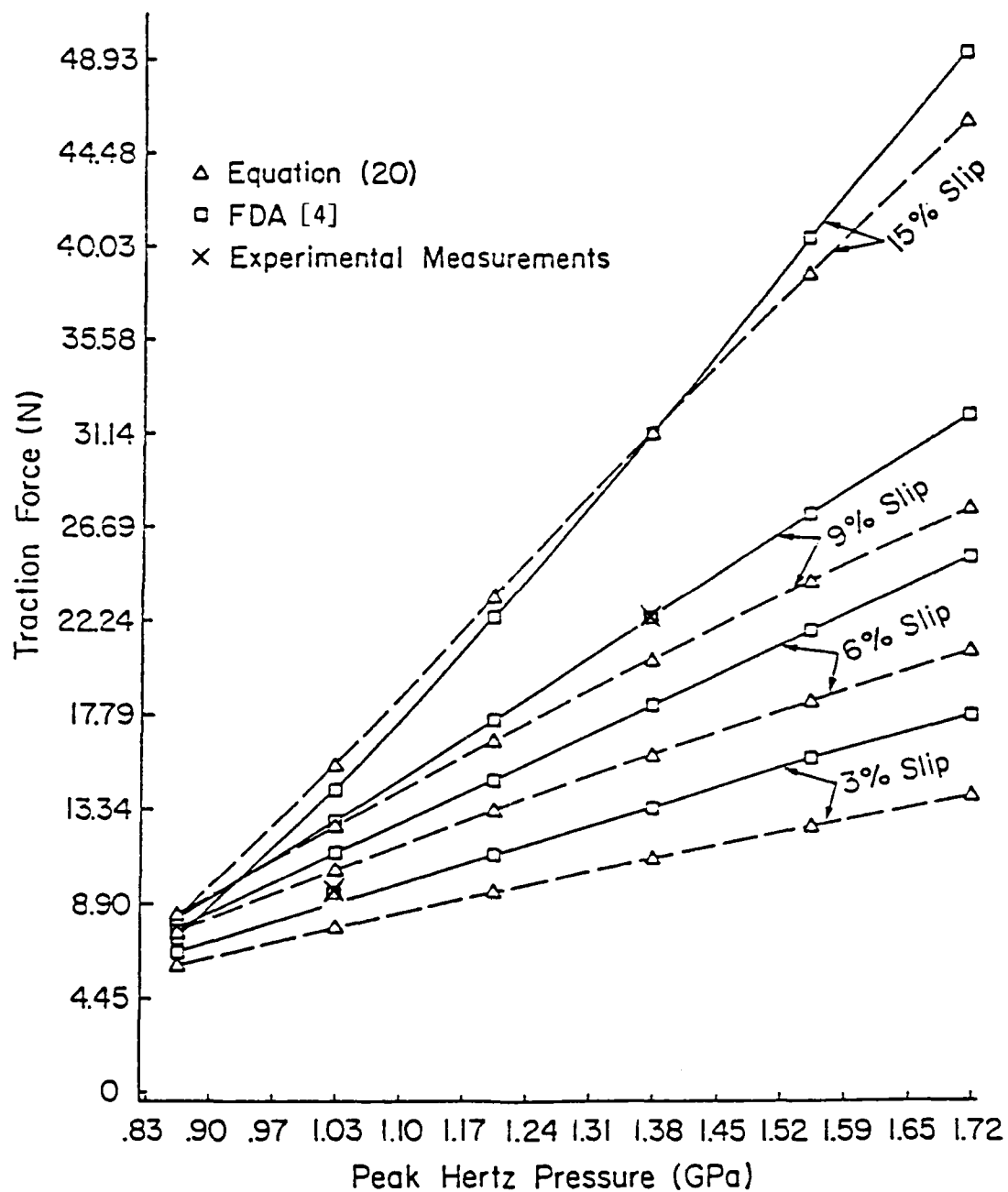


Figure 15. Peak Hertz pressure versus traction force

linear increase. The sliding friction force also increases as the slip ratio is increased. The error between the approximate method obtained from equation (21) and FDA [4] seems to decrease as the sliding velocity is increased. The results from the FDA [4] and an approximate solution correlate very well as illustrated in Figure 15. The maximum error between the FDA [4] and the approximate solution is 14%.

Figure 16 depicts the sliding friction force obtained from the FDA [4] and equation (21) versus sliding velocities at different pressure (loads). The measured sliding friction force at pressures of 1.04 GPa and 1.36 GPa at approximately 6% slip obtained by Dow and Kannel [1] are also depicted. There exists good agreement between the approximate friction force, the measured friction force, and the friction force obtained from the FDA [4]. Equations (21) and (28) could be used as a first step in studying the effects of temperature in EHD lubrication of sliding contacts.

#### Thermoelastic Instability in Elliptic Contact Between Cylinders Under Sliding Contact

The scuffing failure of a sliding contact is a complicated process influenced by surface physics, chemistry, and mechanical science. No comprehensive theory has yet been presented; however, much has been written on this mode of failure. The objective of this (section) is to present a mechanical hypothesis of scuffing failure relating the heat generated due to friction to the resulting distortion of the mating surfaces. From the analysis presented, the conditions for the heating/distortion process to be unstable can be calculated. The analysis relates the influence of load, speed, coefficient of friction, and material properties to the occurrence of unstable thermal conditions which could lead to scuffing failure. The results from this analysis are shown to provide satisfactory agreement with published experimental data.

#### Conceptual Framework

The frictional heating of two bodies in contact causes thermoelastic deformation which may concentrate the heating and greatly increase the contact pressure and temperature. This process can lead to an unstable feedback loop driven by frictional heating and thermal expansion and ameliorated by heat transfer and wear. When this process leads to an unstable increase in contact stress, it is known as thermoelastic instability (TEI). Modern demands for increased performance of sliding systems make the study of thermoelastic instability important.

The idea of a high "flash" temperature in a frictionally heated contact was introduced by Blok [5] and applied by him to explain the failure of lubricated Hertzian contacts as encountered in gearing. Holm [6], Archard [7], and others have drawn upon similar concepts to provide an estimate of localized high temperatures in frictional sliding.

Sibley and Allen [8] carried out a series of experiments on seal materials and developed a criterion for thermal checking and showed

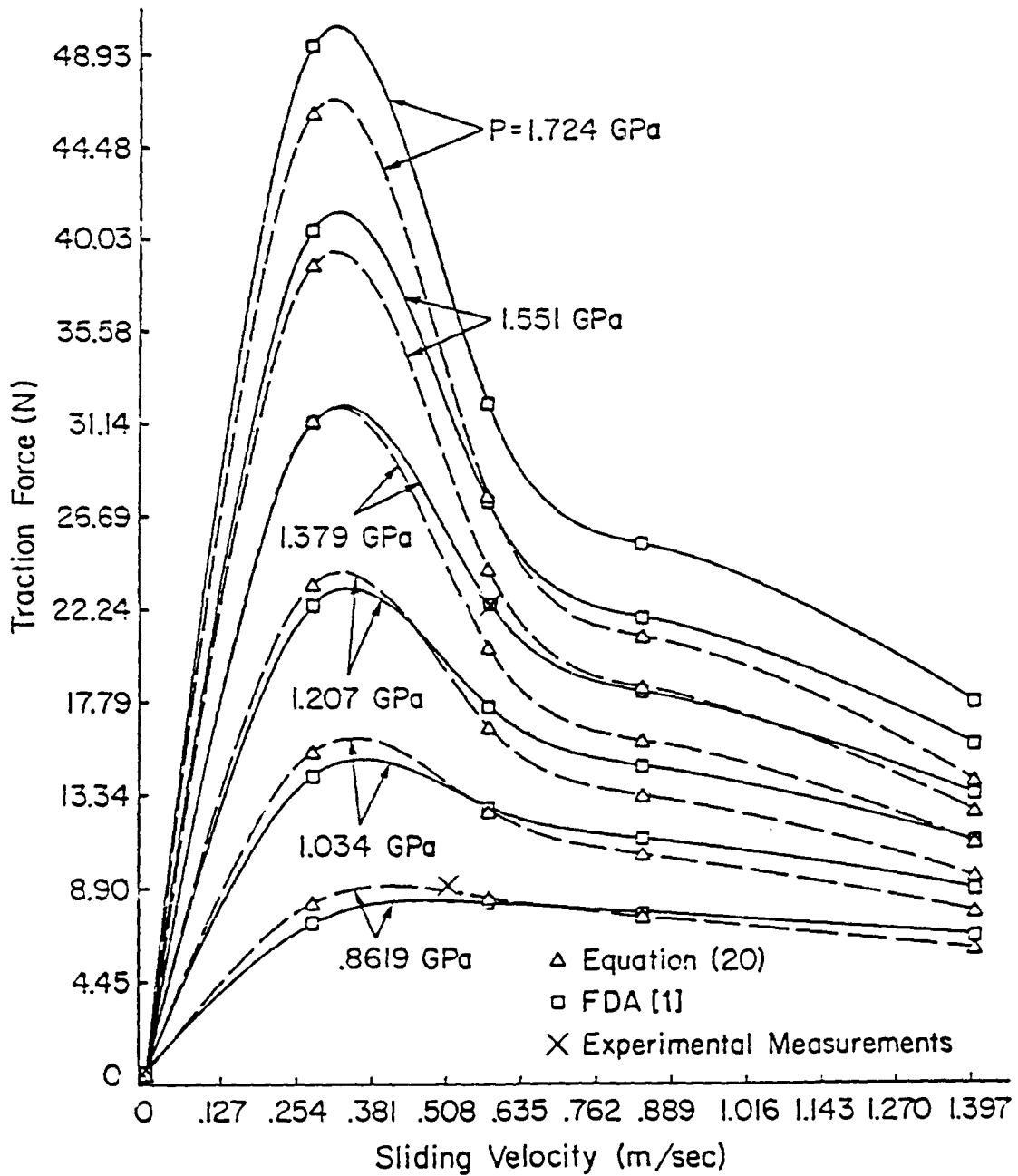


Figure 16. Sliding velocity versus traction force

photographic evidence of systematically moving hot patches in the contact zone. Interest in contact instability and patch formation was accelerated by the work of Barber [9-11] who has demonstrated the phenomenon experimentally and has provided analysis which partially explain his observations as well as making fundamental contributions to the fields of thermoelasticity. His explanations draw upon the modification of asperity contact by frictional heating and wear. His initial interest was the explanation of hot spot effects in railroad brakes.

Dow and Burton [12,13] addressed the 2-D problem of a scraper sliding perpendicular to its edge on a conductive slab and showed that instabilities could be predicted with or without wear. Dow carried out a numerical simulation [14] which predicted the formation and translation of isolated patches and experiments which vividly displayed patch formation [15]. The occurrence of such patches is close to his theoretical critical sliding speed for dry contact, but does not correctly predict the experimental results obtained for wick-lubricated contact. Burton, et. al [16] also demonstrated non-uniform contact exists in seal-like configuration.

Durkee and Cheng [17,18] studied the mechanism of scuffing failure, especially the analytical modelling of the rough elastohydrodynamic problem. They obtained valuable experimental results concerning the load at failure and the sliding speed between the contact of one crowned roller and one cylinder. Sovak and Cheng [19] extended the work to examine the effect of contact geometry on the nature of the initial damage.

From the above survey it can be seen that great progress has been made over the years. However, there is still controversy and a number of unanswered questions for research. The subtlety of the interactions and the difficulties of experimentation are such that the explanation of many important effects is not generally well known and guidelines are not yet available to the designer. This investigation is to establish the theory of thermoelastic instability in the case of elliptic contact of sliding cylinders and to present a simple formulation of the problem to ascertain if it can be used as an estimate for the onset of scuffing failure.

#### Theory and Analysis for a Simplified Case

The influence of thermal expansion on the contact between crowned cylinders is investigated. As shown in Figure 17, the upper cylinder with a crowned surface is stationary and the lower one with the cylindrical surface is rotating.

The Thermally Unstable Condition - Surface irregularities or debris may disturb the pressure distribution by raising the pressure at that point momentarily and cause perturbations of frictional heat input and temperature in the contact area. The growth or decay of the disturbance depends upon heat conduction, thermal deformation and wear. Wear may have some stabilizing effect, but only heat conduction and thermal deformation will be considered here. If the frictional heat generation caused by the pressure perturbation is greater than the heat conducted into the cylinders, heat will accumulate within the contact,

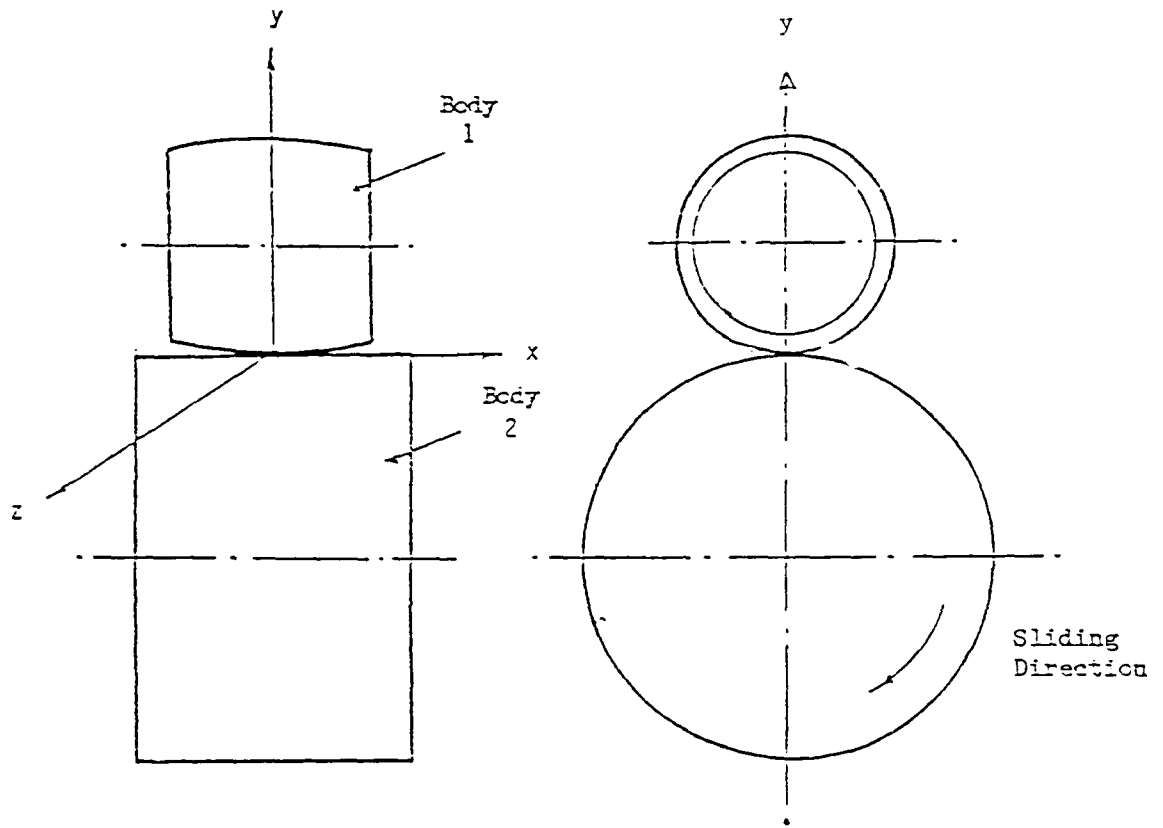


Figure 17. Geometry of the elliptical contact

then the surfaces of the two cylinders will deform further, and the temperature will continue to rise. The heat balance due to the pressure perturbation at the interface is:

$$Q_1 + Q_2 = Q_F \quad (1)$$

where  $Q_1$  is the heat conducted into the stationary cylinder,  $Q_2$  is the heat conducted into the rotating cylinder and  $Q_F$  is the heat generated by friction per unit time.

Heat Conducted by the Stationary Cylinder - The heat conduction equation is:

$$\frac{\partial^2 T}{\partial x^2} + \frac{\partial^2 T}{\partial y^2} + \frac{\partial^2 T}{\partial z^2} - \frac{1}{k_1} \frac{\partial T}{\partial t} = 0 \quad (2)$$

with boundary conditions,

$$T = 0 \text{ at } x = \pm a/2$$

$$T \rightarrow 0 \text{ as } y \rightarrow \infty$$

$$T = 0 \text{ as } z = \pm b/2$$

and equation (1) which is the boundary condition at  $y = 0$ .

With reference to the experiments of Barber [10] and Sibley [8], a temperature disturbance of the following form is selected,

$$T = T_0 F(y) e^{\delta t} \cos \omega_1 x \cos \omega_2 z$$

The  $y$ -dependence of the temperature can be found by substituting this perturbation into the conduction equation. The temperature of the cylinder is then of the form

$$T = T_0 e^{-\alpha y + \delta t} \cos \omega_1 x \cos \omega_2 z \quad (3)$$

where

$$\alpha = \left( \frac{\delta}{k_1} + \omega_1^2 + \omega_2^2 \right)^{1/2} > 0$$

and

$$\omega_1 = \frac{\pi n}{a}, \quad \omega_2 = \frac{\pi n}{b}$$

the conduction in the  $y$ -direction per unit area per unit time is

$$q_1 = -K_1 \frac{\partial T}{\partial y} = K_1 \beta T_0 e^{-\beta y + \delta t} \cos \omega_1 x \cos \omega_2 z \quad (4)$$

The heat input into the surface at that part of the contact area where the temperature is increased can be found by integration over this area, i.e.

$$Q_1 = \iint_{y=0} q_1 \, dx dz = K_1 \beta T_0 e^{\delta t} I_1 \quad (5)$$

where

$$I_1 = \iint \cos \omega_1 x \cos \omega_2 z \, dx dz$$

Heat Carried Away by the Moving Surface - The thermal problem of a heat source moving along a semi-infinite surface has been investigated by Tseng and Burton [20], Barber and Martin-Moran [21] and recently by Gecim and Winer [22]. The following derivation is a straightforward method to get an approximate expression for the heat input.

Since the surface speed is high and the contact area is small, the heat conduction will be considered as one dimensional. The amount of heat passing through  $dx dy$ , a small element of the elliptical contact shown in Figure 18, in unit time [12] is

$$dQ_2 = K_2 T \frac{1}{(\pi k_2 t)^{1/2}} dx dz \quad (6)$$

The time of contact  $t$  can be written in terms of  $z$ , since the sliding velocity is constant.

$$t = \frac{z}{V}$$

Then, at  $y = 0$

$$dQ_2 = K_2 T \left( \frac{V}{\pi k_2 z} \right)^{1/2} dx dz$$

$$Q_2 = K_2 T_0 e^{\delta t} \left( \frac{V}{\pi k_2} \right)^{1/2} I_2 \quad (7)$$

where

$$I_2 = \iint z^{1/2} \cos \omega_1 x \cos \omega_2 z \, dx dz$$

Pressure Fluctuation Due to Heat Disturbance - Assume that the change in shape ( $v$ ) due to thermal deformation can be approximated as a cosine function in the  $xy$ -plane:

$$v = C \cos \frac{\pi}{a} x \quad (8a)$$

and in the yz-plane

$$v = C \cos \frac{\pi}{b} z \quad (8b)$$

where  $a$  and  $b$  are the dimensions of the contact region illustrated in Figure 18 and  $C$  is the amplitude of the perturbation. This change increases the deformation in the center of the contact and reduces it near the edges.

The changes in radius of curvature due to the thermal deformation are defined as:

$$\frac{1}{R_{1t}} = \frac{d^2 v_1}{dz^2} \quad \text{and} \quad \frac{1}{R'_{1t}} = \frac{d^2 v_1}{dx^2}$$

in body 1. Similar changes in radius also occur in body 2. (The  $t$  subscript is related to the changes in geometry due to thermal distortion.) Then from the assumed distorted shape (Equation 8a and 8b), the radii can be related to the original Hertzian contact dimensions.

$$\frac{R'_{1t}}{R_{1t}} = \frac{a^2}{b^2} \quad (9a)$$

$$\frac{R'_{2t}}{R_{2t}} = \frac{a^2}{b^2} \quad (9b)$$

The same result can be obtained if the thermal deformation is expressed as a Fourier series.

The average change in curvature [23] in the central region of the contact (where the pressure is increased) if the surfaces were free to expand due to the heat input is

$$\frac{\partial^2 v_1}{\partial x^2} + \frac{\partial^2 v_1}{\partial z^2} = \frac{(1 + \nu_1)\alpha_1}{K_1} \cdot \frac{Q_1}{\pi ab/4} \quad (10a)$$

$$\frac{\partial^2 v_2}{\partial x^2} + \frac{\partial^2 v_2}{\partial z^2} = \frac{(1 + \nu_2)\alpha_2}{K_2} \cdot \frac{Q_2}{\pi ab/4} \quad (10b)$$

These equations can be used to find the geometrical constants  $A_t$  and  $B_t$ . The increased force ( $P_t$ ) necessary to keep the central part of the surface flat can be found from Hertz equation [24] noting that the positive perturbation width is half the original contact width ( $a$ ).

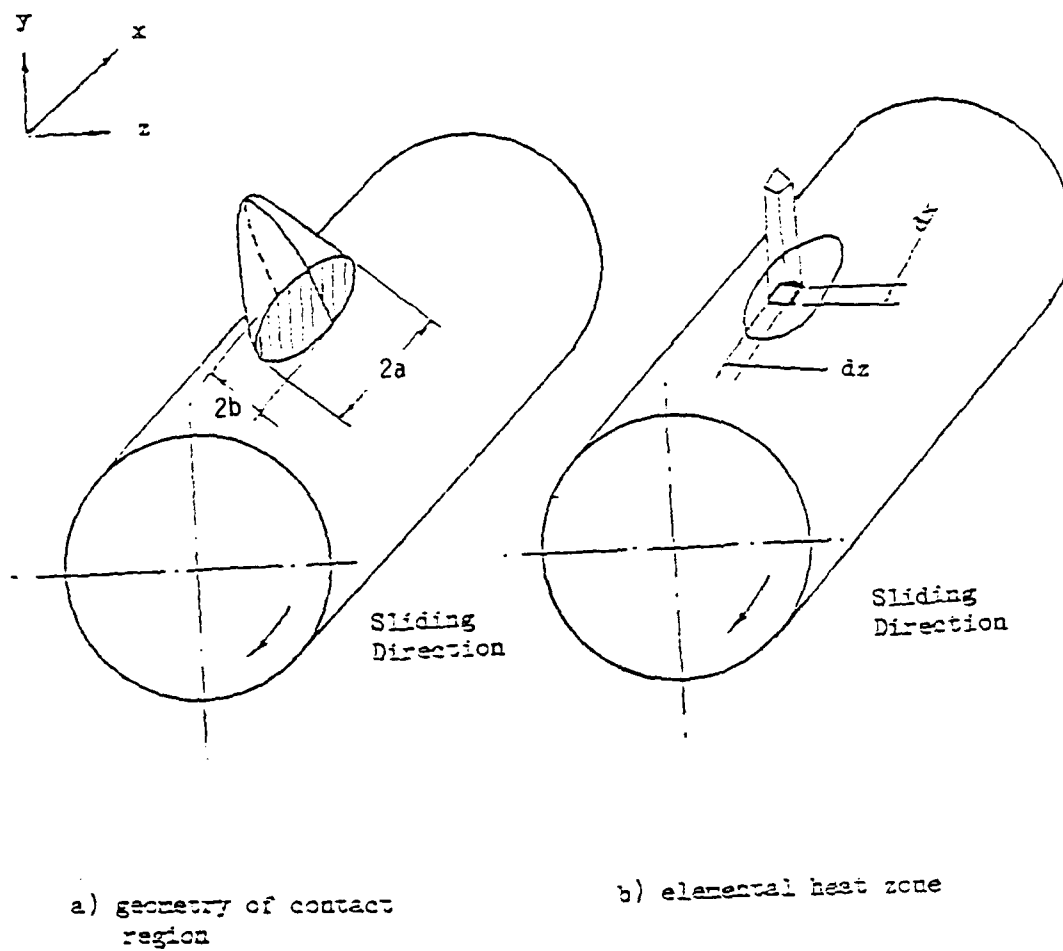


Figure 18. Geometry of contact region showing element of heat transfer analysis

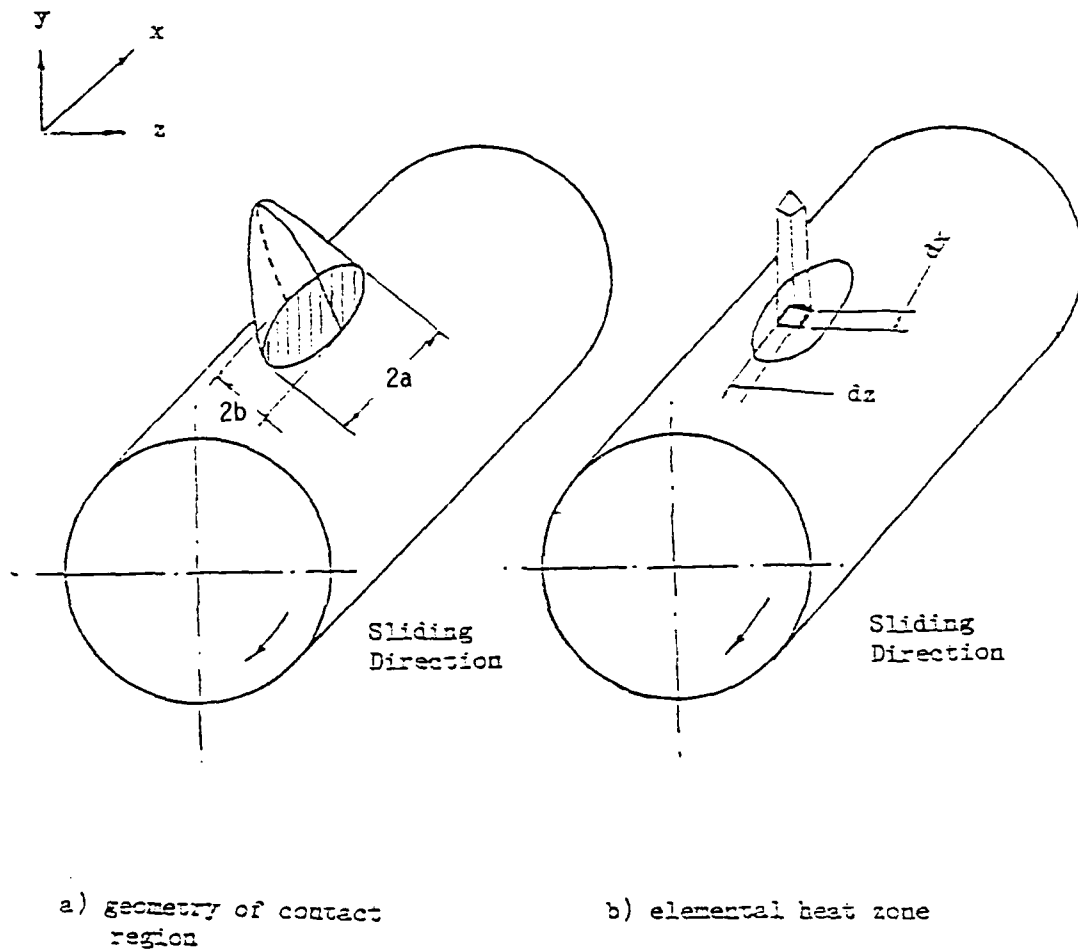


Figure 18. Geometry of contact region showing element of heat transfer analysis

$$P_t = \frac{a^3}{6\pi m_t^3} \left\{ \frac{A_t + B_t}{\frac{1-\nu_1^2}{\pi E_1} + \frac{1-\nu_2^2}{\pi E_2}} \right\} \quad (11)$$

where

$$A_t = \frac{1}{2} \left( \frac{1}{R_{1t}} + \frac{1}{R_{2t}} \right) \quad \text{and} \quad B_t = \frac{1}{2} \left( \frac{1}{R_{1t}} + \frac{1}{R_{2t}} \right)$$

The frictional heat generated by this positive change in force at the center of contact is

$$Q_F = f P_t V \quad (12)$$

There will also be a reduction in load at the outer edge of the contact and reduced heat generation in that region, but that will not lead to an unstable condition.

The Thermoelastic Stability Condition - Substituting equations (5), (7), and (12) into the heat balance equation (1) at the center of the contact, an expression for the thermoelastic stability is obtained.

$$\begin{aligned} \frac{1}{3} \frac{fVa^3}{m_t^3} \frac{1}{\left( \frac{1-\nu_1^2}{E_1} + \frac{1-\nu_2^2}{E_2} \right)} \left\{ (1+\nu_1) \alpha_1 R I_1 + (1+\nu_2) \alpha_2 \left( \frac{V}{\pi k_2} \right) I_2 \right\} \frac{1}{\pi ab} \\ = K_1 R I_1 + K_2 \left( \frac{V}{\pi k_2} \right) I_2 \quad (13) \end{aligned}$$

The above equation gives the relation among load, velocity, coefficient of friction and material properties for the onset of instability. If the materials of the two cylinders are the same:

$$fVa = \frac{6\pi m_t^2 n_t K(1-\nu)}{\alpha E} \quad (14)$$

where  $m_t$  and  $n_t$  are geometric coefficients of the distorted shape from Hertz analysis [24]. Equation (14) gives the value of "a" when the heat balance at the center of the contact is exactly satisfied.

This can be translated to a total system load using equation (11) and the overall geometry of the contact rather than the perturbation geometry. The resulting transition load (W) between stable and unstable operating conditions can then be written as:

$$W = \frac{144 (A + B)}{E^2 (1 - \nu^2)} \left( \frac{\pi m_t^2 n_t^2 K (1 - \nu)}{f V m \alpha} \right)^3 \quad (15)$$

#### Results and Discussion of the Technique Used for the Simplified Case

Equation (15) was evaluated for the case of a crowned steel disk (body 1) in contact with a cylindrical disk (body 2) of the same material. The specific values of the parameters are:

$$\begin{aligned} K &= 14.4 \text{ W/m}\cdot\text{K} & R_1 &= 8.24 \text{ mm} \\ \nu &= 0.3 & R_1' &= 53.2 \text{ mm} \\ E &= 206.8 \times 10^9 \text{ N/m}^2 & R_2 &= 31.7 \text{ mm} \\ \alpha &= 17.3 \times 10^6 / ^\circ\text{C} & R_2' &= \infty \end{aligned}$$

The calculated scuffing loads for different sliding speeds from Equation (15) are plotted in Figure 19 with a range of values for friction coefficient from 0.04. to 0.2 illustrated. A lower friction coefficient (or reduced sliding speed) will result in less heat generation at the interface and therefore less thermal distortion. As a result, a higher load will be required to produce enough distortion for the unstable heating situation to exist; that is, scuffing failure to occur. In the same way, higher values of friction coefficient (or increased speed) will lead to lower scuffing loads.

Also shown in Figure 19 are experimental values of scuffing loads taken from Durkee [17]. These data are for two pairs of steel surfaces with different roughnesses: "smooth" pairs which consisted of a 0.025  $\mu\text{m}$  cla lower surface in contact with a 0.05  $\mu\text{m}$  cla upper surface, and "rough" pairs which consisted of a 0.25  $\mu\text{m}$  cla lower surface in contact with 0.1  $\mu\text{m}$  cla upper surface. These surfaces were lubricated with naphthenic mineral oil. The experimental scuffing loads were strongly influenced by the surface roughness of the mating surfaces. The smooth pairs displayed scuffing loads approximately one order of magnitude larger than the rough pairs at the same sliding speed. Comparing the experimental results to the corresponding constant friction coefficient curves from the analysis indicates a value of  $f$  less than 0.1 for the smooth pairs and approximately 0.2 for the rough surfaces.

The maximum Hertzian stress for the elliptical contact is shown in Table 3 for loads from 200 to 1000 N (45 to 225 lbs).

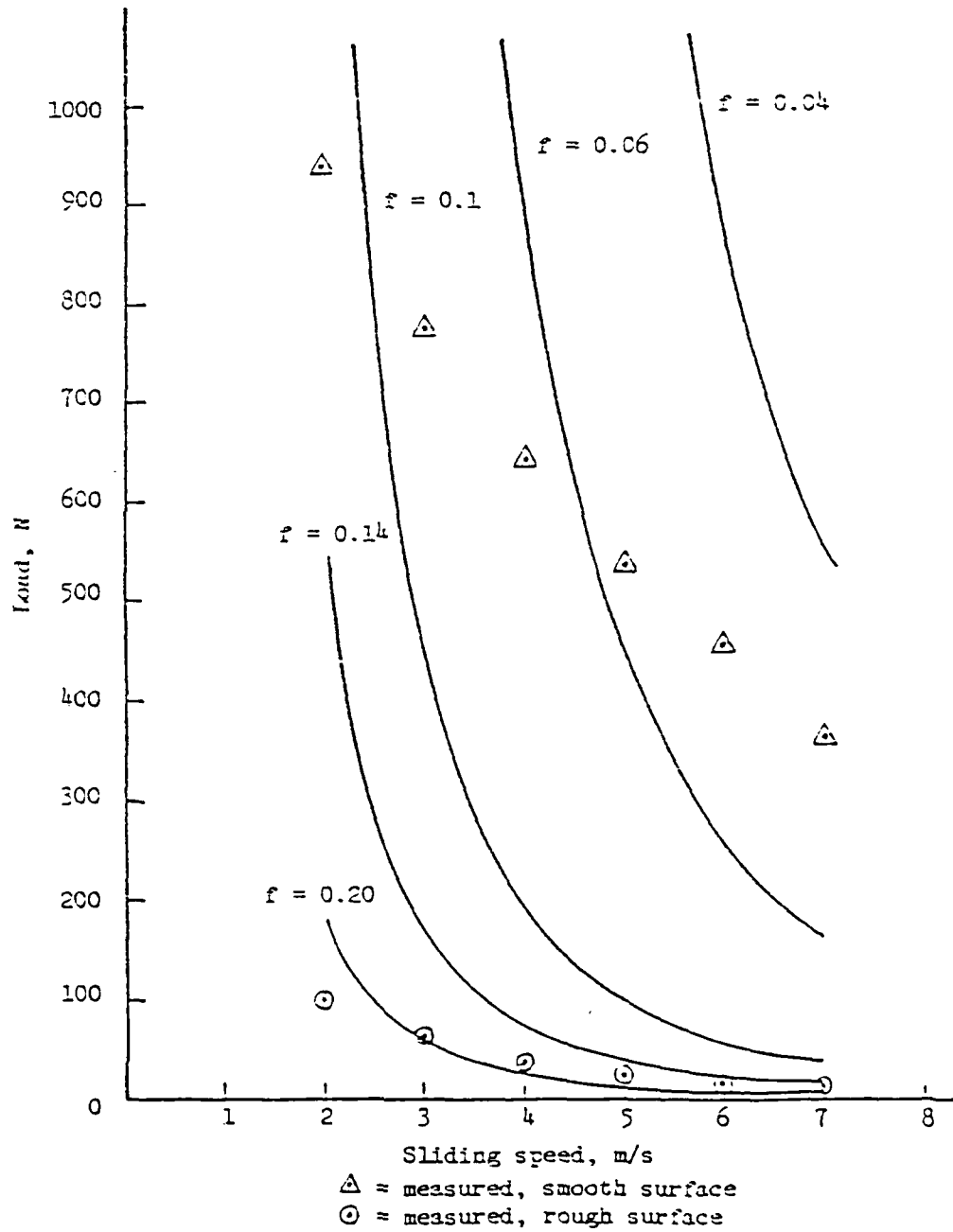


Figure 19. Comparison of calculated and measured [17] scuffing loads for smooth and rough surfaces

Table 3 Contact geometry for different normal loads

Load, N	Half-width of contact, mm	Half-length of contact, mm	Maximum Hertzian Stress, GPa
200	0.548	0.139	1.26
400	0.691	0.175	1.58
600	0.791	0.200	1.81
800	0.870	0.220	2.00
1,000	0.938	0.237	2.15

The elastohydrodynamic film thickness for these conditions (high contact stress and pure sliding) will be extremely thin and thus contact of the surface asperities will most certainly occur. This would explain the higher apparent friction coefficient for the rough surfaces. An increase in roughness would be accompanied by more asperity contacts, smaller percentages of the load supported by the fluid film, and higher friction force. EHD film would also explain the apparent reduction in friction coefficient for the smooth surfaces as the speed is increased. Higher speeds will generate a thicker film and a net decrease in friction force. Therefore, to predict the boundary of the stable region, that is the scuffing load, an independent expression for friction coefficient must be used.

An estimate of the friction coefficient [25] in the mixed lubricated regime is:

$$f = 0.0127 \log_{10} \left( \frac{3.17 \times 10^8 W/L}{u(V_1 - V_2)(V_1 + V_2)^2} \right) \quad (16)$$

where  $V_1$  and  $V_2$  are in in/s,  $W/L$  load per unit width in lb/in, and  $u$  the absolute viscosity in centipoise. In the elliptic contact of smooth surfaces, an equivalent load  $W/L$  is used in this equation. The equivalent load per unit length is that load which produces the same Hertzian contact stress in the line contact of two cylinders as that in the elliptic contact case.

In the case of rough lubricated surfaces, the coefficient of friction at  $V = 4.15\text{m/s}$  is chosen as 0.14 from experimental results [17]. The coefficient of friction at other speeds is calculated in proportion to  $f = 0.14$  by means of Equation (16) with constant values of  $W/L$  and  $u$ . The coefficient of friction thus obtained is shown in Table 4.

Table 4 Friction coefficient [21] for sliding surfaces

Speed	2 m/s	3 m/s	4 m/s	5 m/s	6 m/s	7 m/s
f (smooth)	0.068	0.060	0.055	0.051	0.048	0.045
f (rough)	0.158	0.148	0.140	0.134	0.129	0.126

Figure 20 illustrates the agreement between the measured scuffing loads and the theoretical predictions of thermally unstable contact regions. In general the agreement is quite good; in most cases, the differences between calculated and measured limiting speeds are below 30%. The difference at high load is large, reaching 72% at 940N load. The cause could be that the friction coefficient in that case (0.068) may be too low. Lubrication is poor at low speed and high load and Equation (16) may not predict the value under these conditions.

#### Experimental Testing of Failure Due to Scuffing

##### Apparatus Design

The main parts of the experimental equipment are two disks in contact. The upper disk is 45 mm in diameter with a crown radius of 140 mm. The lower disk is cylindrical: 60 mm in diameter and 85 mm in length. This cylinder is supported by two ball bearing, and is driven by a 3 HP variable speed motor through a V-belt drive. The runout of the cylinder is below 13  $\mu$ m. A belt drive is used to get a maximum speed of 3000 RPM. The highest speed used in the experiment has been 2100 RPM. A reduction belt drive is used at speeds below 1000 RPM to get sufficient torque by changing the pulleys of the belt drive. The upper disk is also supported in ball bearings located in the case with a load arm on either end. In the present experiments, the upper disk is held stationary by the friction measurement device. Modifications may be made utilizing measuring and controlling devices, to allow, the upper disk to rotate during the tests.

After each test, both the surfaces of the upper and lower disks are either damaged or worn. New regions on the two disks are brought into contact for the next test by moving the upper disk axially a certain distance along the cylinder. Because the upper disk does not rotate, it can be moved through a small angle to get a new part of surface on the upper disk into the contact region.

The load is applied by hanging weights on the end of the load arm. A counterbalance load is fixed on the other side of the load arm. Weights are suspended on this end of the arm so as to counterbalance the weight of the upper disk and the load arm on the other side. Thus, there is no force between the two disks when no weight is hung on the load arm. The maximum force applied on the contact is 2100 N (465 lb.) when weights of 147 N (33 lb.) are hung on the load arm.

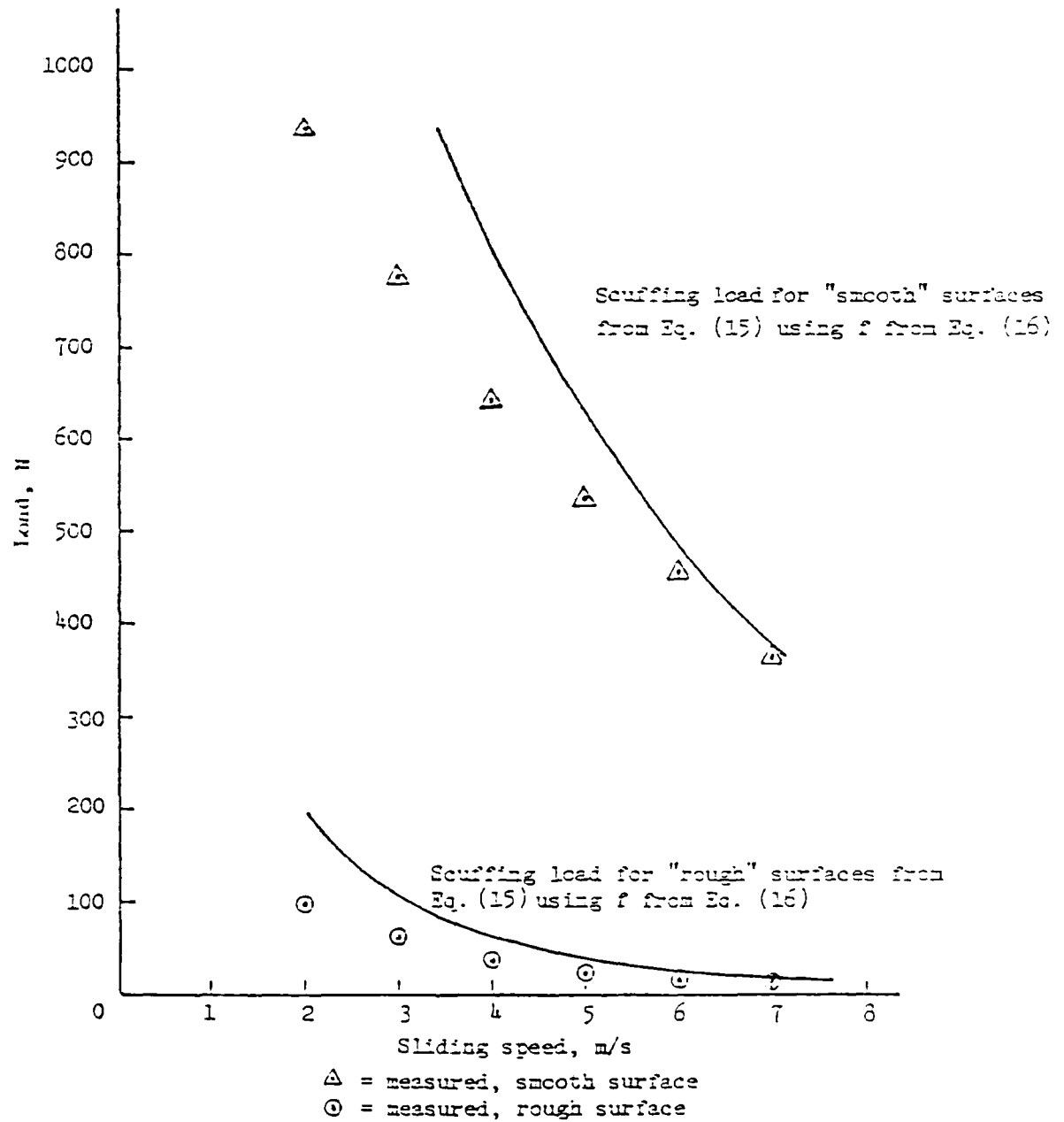


Figure 20. Comparison of calculated and measured [17] scuffing loads with friction coefficient calculated from Eq.

The rotation speed is measured by means of a toothed gear and a transducer. The gear with 60 teeth is fixed on one end of the shaft of the lower cylinder. The displacement transducer is placed near the gear and the output is sent to a frequency counter which indicates the rotation speed.

Solenoids are placed under the load arm to facilitate releasing the load by pushing the load arm upward at the instant when surface failure occurs. The solenoids can be triggered by the temperature rise, or the friction increase, or the vibration produced. The vibration level as measured via an accelerometer was found to be the best indicator of scuffing failure.

Temperature in the contact area of the two disks during sliding is sensed by an infrared thermo-monitor (Vanzetti model 3025) and is displayed on an oscilloscope. The response of the infrared thermometer is fast and no temperature gradient is produced as in the case of thermocouple, so it is more effective in monitoring transient temperature. The spot size of the focused light is about 1.0 mm and the distance of focus is 38 mm. Unfortunately, the infrared thermometer can only sense relatively high temperature; the minimum temperature sensed is about 80° C. The purpose of this research is to investigate the temperature rise during scuffing of a sliding contact; this temperature is typically above 80° C. If the contact temperature is below 80° C, the scuffing regime has not been reached.

The friction force produced in the contact during sliding is measured by the device which is fixed on the shaft of the upper disk. The friction force tends to rotate the upper disk and with it a bar which is clamped on the shaft of the upper disk. The bar compresses a spring and changes the small gap between the surfaces of an eddy current proximity sensor and the bar, and an output proportional to the traction force is detected.

The bolt on the side of the spring is used to adjust the gap between the transducer and the bar and the preload of the spring. The diameter of the bolt hole is made bigger than that of the bolt, so the bar is free to rotate without constraint. The hook on the bar is used to attach a wire for hanging weights during calibration. The wire passes through pulleys which are clamped on the base of the test rig only at the time of calibration. On the other end of the wire, weights of known magnitude are hung. At the same time readings of voltage on the oscilloscope are taken. Thus, the relation between force and voltage reading can be found.

The cylinder and the disk are lubricated by a wick system. A basin is placed under the lower cylinder with oil poured in it. Some pieces of felt are fixed on the bottom of the basin. The felt touches the lower surface of the cylinder. When the cylinder turns, sufficient oil is carried on the surface of the cylinder into the contact region.

Test Procedure - During the test, the speed of the lower cylinder is adjusted to the desired rotating speed. A certain amount of load is added to the load arm and the test is run for this load from the

beginning to the end. If scuffing failure occurs, temperature, friction and vibration increase steeply and simultaneously. At this point the solenoids are activated and the load arm is pushed up to separate the two contact surfaces and the test stops. If failure does not occur, the test is run for about 60 seconds and then is stopped. A sequence of tests are run in which the load is either less than the previous test, or larger, depending on whether there was failure or not. The tests are continued until the threshold of scuffing load is obtained.

The scuffing tests were run in groups according to the combination of lubricant and disk material used. Each group consisted of approximately 35 scuffing tests which were run over the load and speed ranges of the apparatus. The following is a listing of the test groupings:

#### Test Group 1

- lubricant: XRM-109 synthetic paraffinic oil, viscosity = 447 cStokes at 40 C
- roller material: 52100 alloy steel, hardness Rc 60
- calculated specific film thickness ( $\lambda$  ratio): 5 to 8

#### Test Group 2

- lubricant: Mobil SHF-61, synthetic base stock, viscosity = 28 cStokes at 40 C
- roller material: 52100 alloy steel, hardness Rc 60
- calculated specific film thickness ( $\lambda$  ratio): 0.4 to 1.3

#### Test Group 3

- lubricant: Mobil SHF-401, synthetic base stock, viscosity = 443 cStokes at 40 C
- roller material: 52100 alloy steel, hardness Rc 60
- calculated specific film thickness ( $\lambda$  ratio): 4 to 12

#### Test Group 4

- lubricant: Mobil SHF-401, synthetic base stock, viscosity = 443 cStokes at 40 C
- roller material: 440C0 stainless steel, hardness Rc 60
- calculated specific film thickness ( $\lambda$  ratio): 7 to 20

The following parameters were either determined or set prior to a test: geometry of contact, surface roughness of contact, load, speed, lubricant, and roller material. The parameters measured during a test were: frictional force, vibration, temperature, and time to failure.

The sequence of tests within a test group generally depended upon whether failures had occurred during the first several tests. If a failure had occurred, either load or speed was reduced in subsequent tests until a non-failure was observed. If a failure did not occur initially, load or speed was increased in each subsequent test until failure occurred. Each test was run on a new, un-worn spot on the fixed disk and on a new un-worn track on the rotating disk. In this way, a failure boundary was defined. The choice as to whether to vary load or speed depended upon the region of the theoretical fV curve being explored. At high speeds and low loads, the curve predicts insensitivity to further changes in speed. At high loads and low speeds, the curve predicts insensitivity to further changes in load.

### Experimental Results

The theoretical scuff boundary curves presented herein were used to evaluate the results of the experiments and to correlate them with the theory. The theory would be shown to be ideally valid if all non-failures occurred in both plots on the side of the boundary closest to the ordinate. Conversely, scuffing failures would ideally occur on the opposite side of the boundary.

The intent of each test group was to evaluate the response of the model for a different lubricant-metal combination; therefore, the results are presented by test group. A plot is given for each test group: load versus heat generation,  $Q = fVL$ . In each of the figures, failures are indicated by circles and nonfailures are indicated by squares. The theoretical boundary is shown by a solid line.

The data of group 1 (Figure 21) correlates with the theoretical prediction of the failure boundary, in that most of the experimental test results occurred on the side of the boundary for which they were predicted to occur. The uncertainty band of  $\pm 10\%$  is included in the figure.

Group 2 results (Figure 22) show a marked difference from the results of Group 1 in that no correlation with the predicted failure boundary is apparent. The difference between the two test groups was the contact lubricant used. SHF-61 is much less viscous than XRM-109. Reduction of lubricant viscosity reduces the film thickness in the contact and alters the coefficient of friction, resulting in scuffing failure under less severe loads and velocities. For this group of tests  $\lambda$  lies in the range of 0.4 to 1.3. The results indicate that the theory does not adequately predict the scuffing boundary in this range of calculated specific film thickness. In addition, the calculated  $\lambda$  ratios indicate a high degree of asperity contact, suggesting that the heat generation in these tests is due to solid contact, rather than shear in the lubricant. The theoretical model is not affected by this distinction, however, because it is formulated on the basis of an overall friction coefficient  $f$ .

Since the data of Group 2 do not correlate with the predicted failure boundary, the question arises, can a failure boundary be determined for this set of data? One may speculate that the scuffing boundary curve of the model could be modified empirically to account for a change in the calculated specific film thickness. It is apparent that the actual failure boundary is less than the predicted boundary. This implies a modification of the coefficient of friction in the model formulation to suitably account for lower calculated specific film thickness. It is also possible that in this lower specific film thickness regime another failure mechanism is present -- namely that described by Snidle, Rossides and Dyson [26].

Test results for Group 3 are similar to those of Group 1, as expected, since the lubricants are very similar. Figure 23 illustrates that the results correlate with the theoretical failure prediction.

The objective of the experiments of Group 4 (Figure 24) was to test the response of the model to change in thermal properties ( $K, \alpha$ ), although the material properties ( $E, \nu$ ) also vary when the disk material is different. The tests were run in the high calculated  $\lambda$  ratio regime, since correlation with theory had already been observed.

The results show correlation with the theoretical failure boundary, in support of the theoretical model. A comparison between results of Group 3 and 4, in which the disk material was the only significant variable, shows that the experimental results do not answer the question as to whether there is a difference or not.

There exist two possible explanations for this result. One explanation lies in the possibility that the friction force measurement was not sensitive enough to detect a difference. An interesting experimental observation clouds this conclusion, however. As described earlier, a sequence of tests was run at either constant load or speed to define the experimental failure boundary. This is observable in each of the plotted figures if one follows a line of constant load, for example, across a plot. In many cases, despite an incremental increase in speed, a jump in the magnitude of  $Q$  occurred across the failure boundary. The jump was large compared to the instrument resolution capability and it indicates that an increase in sensitivity might not increase the definition of the failure boundary, and that the scuffing boundary might be thought of as a band rather than a line, as predicted by theory.

The second explanation is that the response of the model to variation in thermal and material properties, although theoretically predicted, may be masked in actual observation by other mechanisms or processes not adequately addressed by the model.

#### Time Dependency of Failure

The time to failure does not appear to correlate to any particular quantity over the test groups, but is a trend observable within a test set. That is, within a set of tests in which the paired surface roughnesses did not change, a failure generally occurred after longer period of running (or not at all) if the load and/or speed was reduced. The

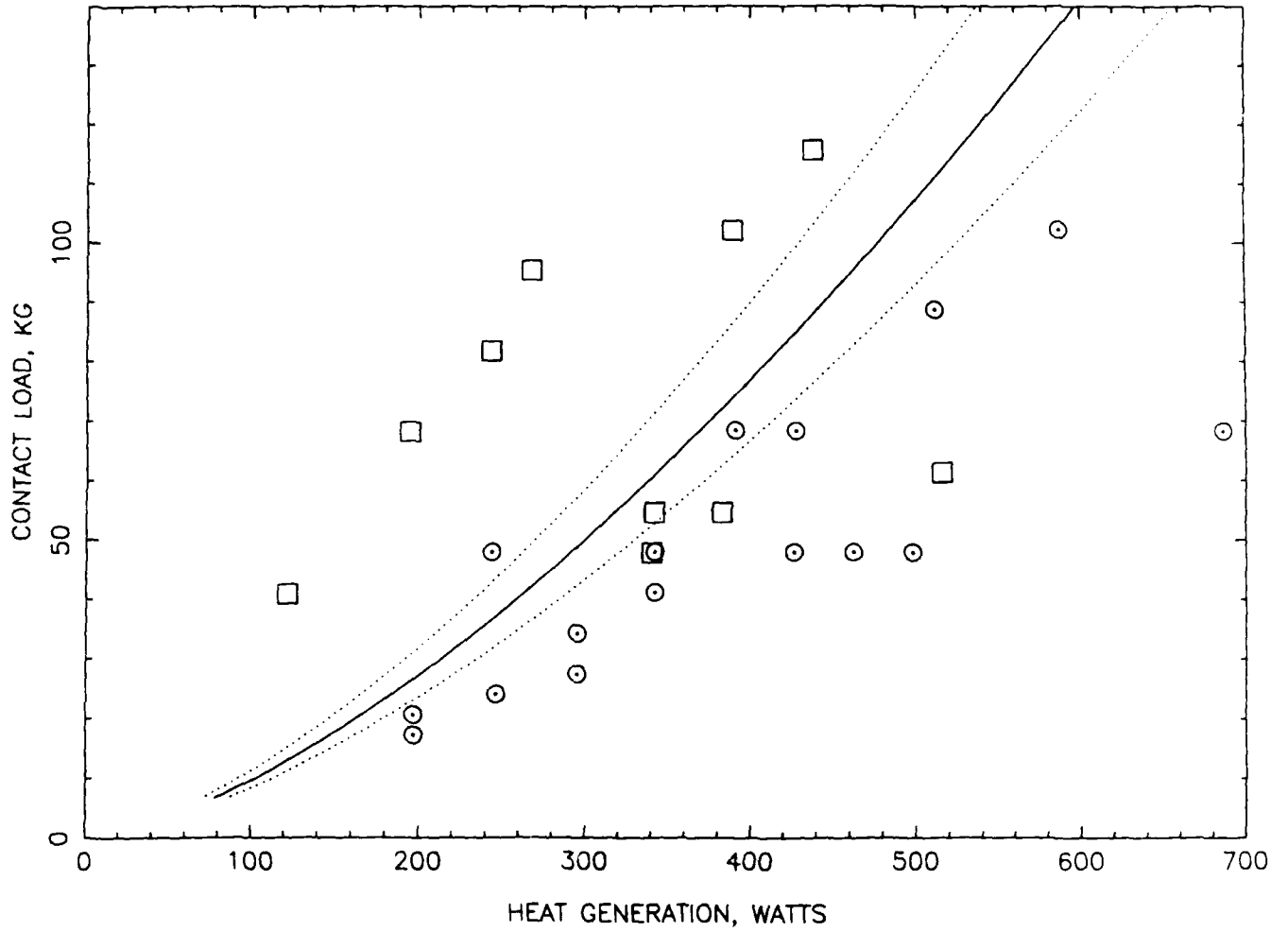


Figure 21. Results of Test Group 1: lubricant XRM-109, disk material 52100 steel,  $5 < \lambda < 8$ ; circles indicate scuffing failures, squares indicate non-failures.

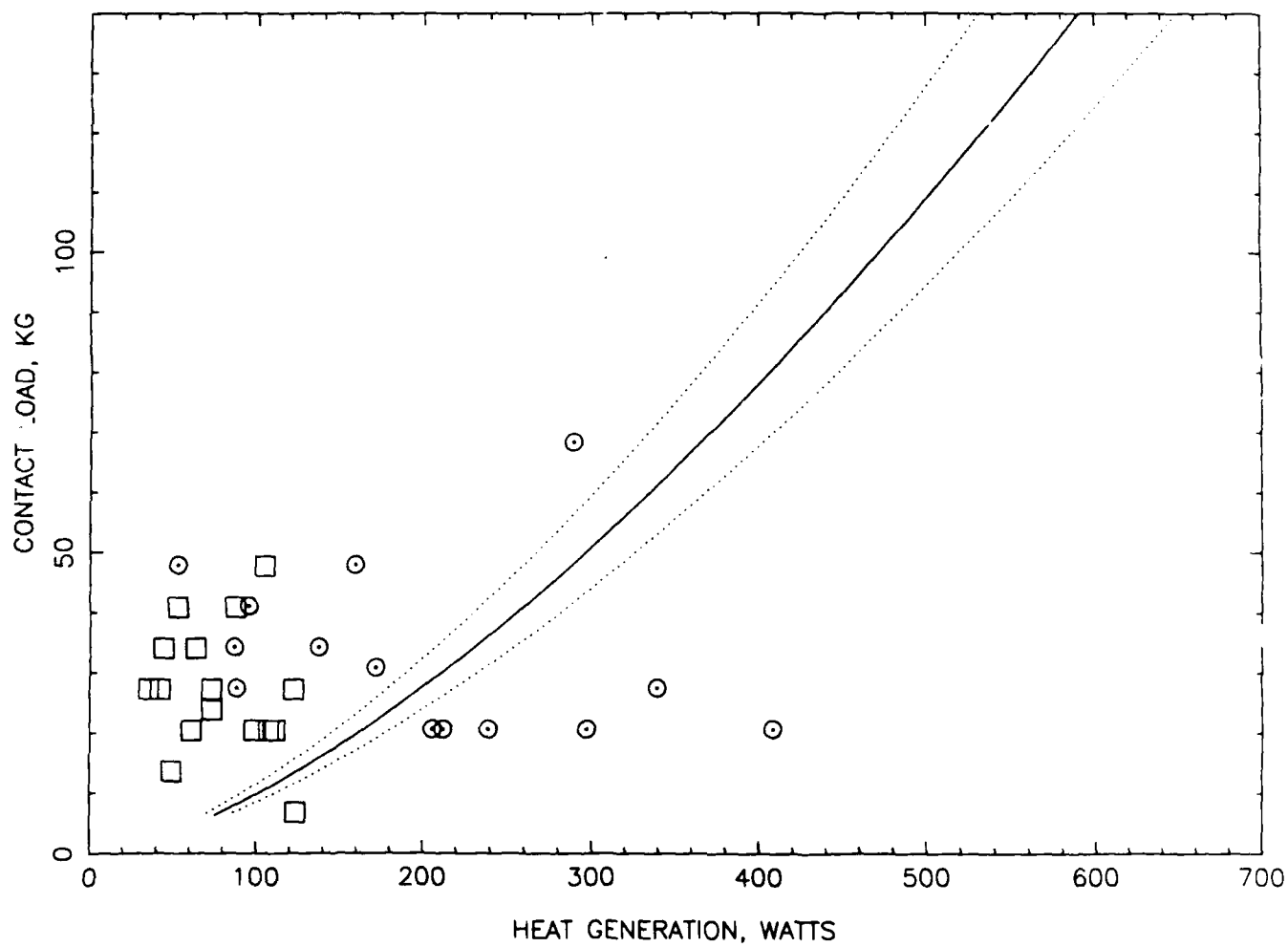


Figure 22. Results of Test Group 2: lubricant SHF-61, disk material 52100 steel,  $0.4 < \lambda < 1.3$ ; circles indicate scuffing failures, squares indicate non-failures.

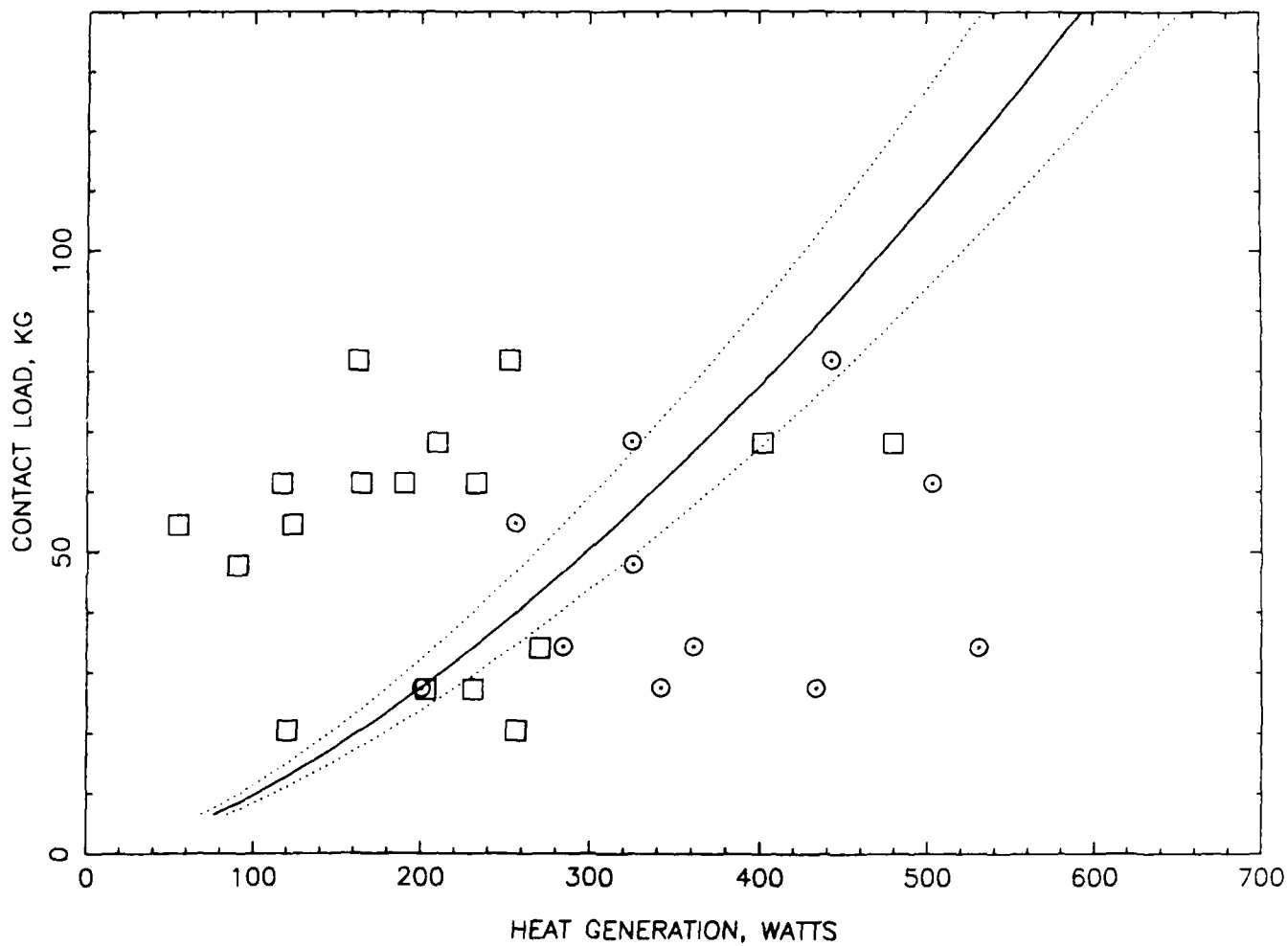


Figure 23. Results of Test Group 3: lubricant SHF-401, disk material 52100 steel,  $4 < \lambda < 12$ ; circles indicate scuffing failures, squares indicate non-failures.

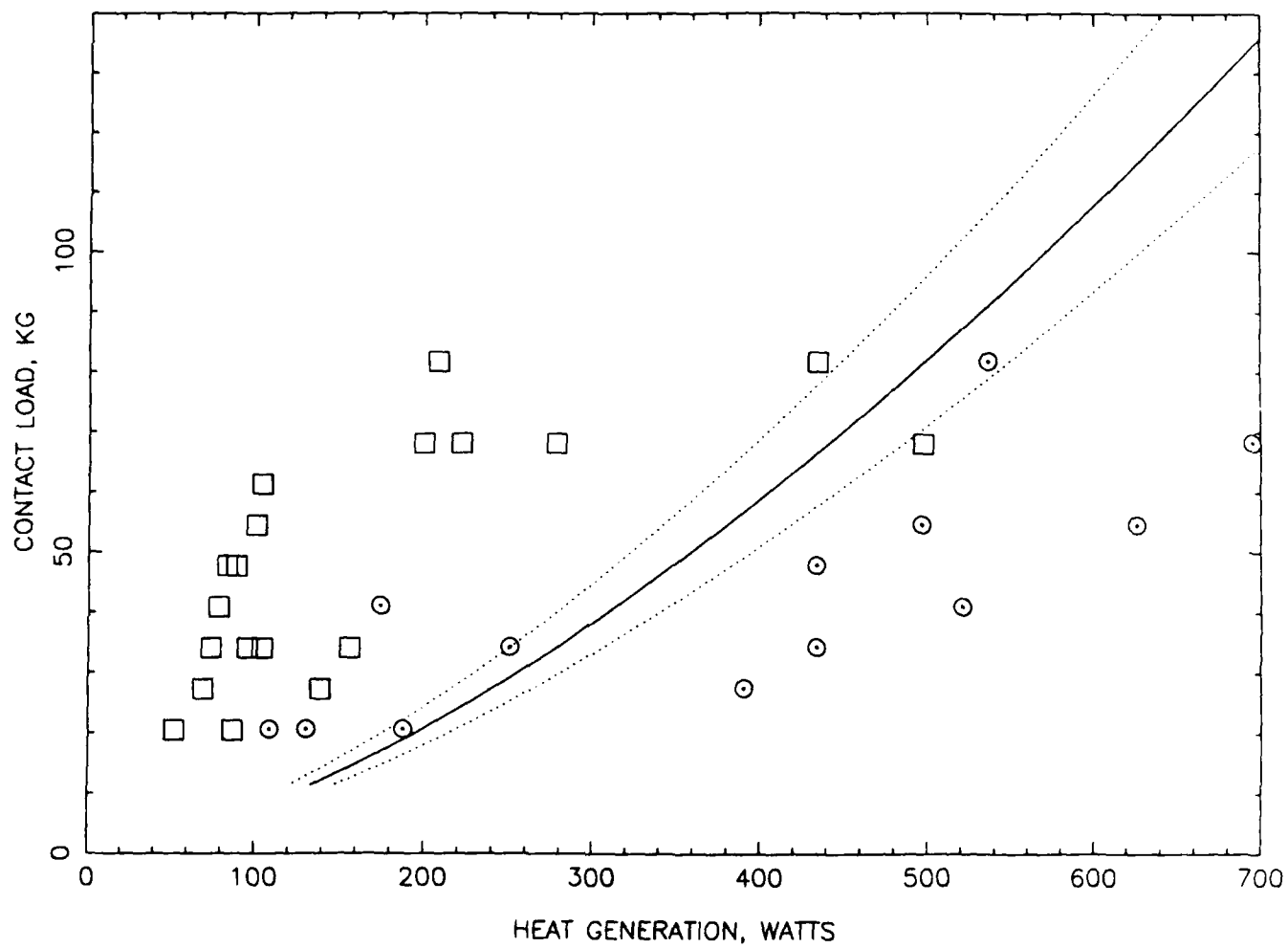


Figure 24. Results of Test Group 4: lubricant SHF-401, disk material 440C stainless steel,  $7 < \lambda < 20$ ; circles indicate scuffing failures, squares indicate non-failures.

actual test duration and load/speed relationship was not consistent between test sets.

This general trend was observed in test Groups 1,3 and 4. Test duration in Group 2, in which the calculated  $\lambda$  ratio was significantly lower, did not follow the described trend. Failures generally occurred within the first minute, or not at all. Most failures occurred in the first few seconds of running.

These observations are in agreement with Durkee's research [18], in which scuffing experiments were run for two ranges of surface finish. Durkee observed a time dependency of failure for the "smoother" tests and immediate failure for the "rough" tests. Although Durkee does not present specific film thickness values, it may be inferred that the tests run on smooth surfaces correspond to larger  $\lambda$  ratios, relative to the tests run on rough surfaces.

#### Wear Observations

Throughout the scuffing experiments, wear was visible on both cylinders for tests in which failure did not occur. This was an unexpected result, since calculated specific film thickness predicted little or no asperity contact in test Groups 1,2 and 4. The disparity between observed wear and  $\lambda$  ratio calculations is attributed to the calculation model, which does not consider heating due to slip in the contact.

The weld patterns left on the lower cylinder from scuffing failure were observed to form a track which was slightly helical about the cylinder axis, suggesting that failure occurred at one point in the contact region, and traversed the contact as material was lost to the rotating cylinder. This correlates to the moving hot spots described in studies by Dow 13. The dimensions of the wear markings left on the upper cylinder when a failure did not occur were measured and found to compare closely with the calculated Hertzian dimensions.

#### Effects of Experimental Uncertainty

Although the frictional force measurement contained a relatively large uncertainty, the effect of this is minimized in light of the most important determination -- that is, prediction of failure. How near or far away a test point lies to the predicted boundary is of secondary importance. In most cases, an uncertainty of  $\pm 10\%$  in the frictional force does not alter which side of the boundary a test point lies. It is interesting to note that relatively few data points were actually found to lie in proximity to the boundary, although considerable effort was made to obtain data in the boundary region.

## REFERENCES

1. Kannel, J. W. and T. A. Dow, "The Relation between Pressure and Temperature in Rolling/Sliding EHD Contact," Journal of American Society Lubrication Engineers, Trans. ASME, Vol. 23, No. 3, pp. 262-268, 1979.
2. Roelands, C. J. A., J. C. Vlugter, and H. I. Watermann, "The Viscosity of Temperature Pressure Relationship of Lubricating Oils and Its Correlation with Chemical Constitution," Journal of Basic Engineering, pp. 601-606, 1963.
3. Sadeghi, F., "Analysis of Thermal Elastohydrodynamic Lubrication in Rolling/Sliding Contact," PhD Thesis, North Carolina State University, Raleigh, 1985
4. Sadeghi, F. and T. A. Dow, "Thermal Analysis of Elastohydrodynamic Lubrication in Rolling/Sliding Contacts," Journal of Tribology, Trans. of ASME, Vol 109, 1987.
5. Blok, H., "Theoretical Study of Temperature Rise at Surface of Actual Contact Under Oiliness Lubricating Conditions," General Discussion on Lubrication, Inst. Mech. Eng. Vol. 2, 1937, pp. 222-235.
6. Holm, R., "Calculation of the Temperature Development in a Contact Heated in The Contact Surface and Application to the Problem of the Temperature Rise in a Sliding Contact," Journal of Applied Physics, Vol. 19, 1948, pp. 361-366.
7. Archard, J. R., "The Temperature of Rubbing Surfaces," WEAR, Vol. 2, 1959, pp. 438-455.
8. Sibley, L. B., and C. M. Allen, "Friction and Wear Behavior of Refractory Materials at High Sliding Velocities and Temperatures," ASME Paper No. 61-Lub-15.
9. Barber, J. R., "Thermal Effects in Friction and Wear," Dissertation, Cambridge University, 1968.
10. Barber, J. R., "Thermoelastic Instabilities in the Sliding of Conforming Solids," Proc. Roy. Soc., Ser. A., Vol. 312, 1969, pp. 381-391.
11. Barber, J. R., "The Influence of Thermal Expansion on the Friction and Wear Process," WEAR, Vol. 10, 1967, pp. 155-159.
12. Dow, T. A. and R. A. Burton, "Thermoelastic Instability of Sliding Contact in the Absence of Wear," WEAR Vol. 19, 1972, pp. 315-328.
13. Dow, T. A. and R. A. Burton, "The Role of Heat in the Initiation of Thermoelastic Instabilities of Rubbing Contact," ASME Journal of Lubrication Technology, Vol. 95, 1973, pp. 71-75.

## APPENDIX A

Participants

T. A. Dow, Prof. NCSU  
 R. R. Johnson, Assoc. Prof. NCSU  
 T. G. Bifano, Research Engineer, NCSU  
 Y. Y. Zhang, Visiting Assoc. Prof., NCSU  
 F. Sadeghi, Grad. Student, NCSU, (currently Asst. Prof. Purdue University)  
 J. Rhatigan, Grad. Student, NCSU (currently at NASA - Lewis)  
 W. Larson, Grad. Student, NCSU

Papers Submitted for Presentation and Publication

1. Sadeghi, F. and Dow, T. A., "Thermal Effects in Rolling/Sliding Contacts: Analysis of Thermal Effects in Fluid Film," Journal of Tribology, Trans. ASME, Vol. 109, pp. 512-518, July 1987.  
 Also presented at ASME/STLE Tribology Conference, Pittsburgh, PA, 1986.
2. F. Sadeghi, T. A. Dow, and R. R. Johnson, "Thermal Effects in Rolling/Sliding Contacts: Approximate Method for Prediction of Mid-Film Temperature and Sliding Friction," Journal of Tribology, Trans. of ASME, Vol. 109, pp. 519-524, July 1987.  
 Also presented at ASME/STLE Tribology Conference, Pittsburgh, PA, 1986.
3. Johnson, R. R., Dow, T. A., and Zhang, Y. Y., "Thermoelastic Instability in Elliptic Contact Between Two Sliding Cylinders," Journal of Tribology, Trans. of ASME, Vol. 10, No. 1, pp. 80-86, Jan. 1988.  
 Also presented at ASME/STLE Tribology Conference, San Antonio, TX, 1987 (Paper 87-Trib-59).
4. Rhatigan, J., Johnson, R. R., and Dow, T. A., "An Experimental Study of Thermoelastic Effects in Scuffing Failure of Sliding Lubricated Contacts," Submitted to Journal of Tribology, Trans. ASME. Accepted for presentation at ASME/STLE Tribology Conference, Baltimore, MD, 1988.

Degrees Granted

F. Sadeghi, PhD. Dissertation Title: Analysis of Thermal Elastohydrodynamic Lubrication in Rolling/Sliding Contacts, 1985.

J. Rhatigan, MS. Thesis Title: Experimental Study of Thermoelastic Effects in Scuffing Failure of Sliding Lubricated Contacts.

MED  
8